

1 **Non-peer reviewed EarthArXiv preprint**

2 **The Paleozoic Central Patagonian Igneous Metamorphic Belt: its geodynamic**
3 **and tectonic interpretation based on Paleogeographic reconstructions**

4 Haroldo Vizán^{1, 2, *}

5 **1.** Instituto de Geociencias Básicas, Aplicadas y Ambientales de Buenos Aires
6 (IGEBA, CONICET-UBA).

7 **2.** Departamento de Ciencias Geológicas. Facultad de Ciencias Exactas y Naturales,
8 Universidad de Buenos Aires. Intendente Güiraldes 2160, C1428EHA Ciudad
9 Autónoma de Buenos Aires, Argentina.

10

11 *Corresponding author, vizan.haroldo@gmail.com, haroldo@gl.fcen.uba.ar

12

13

14

15

16

17

18

19

20

21

22

23 **Non-peer reviewed EarthArXiv preprint**

24

25 **Abstract:** In the southwestern margin of the North Patagonian Massif there is a NW-
26 SE belt of igneous and metamorphic rocks defining a limit between the North
27 Patagonian Massif and southern Patagonia (including the Deseado Massif), named the
28 Central Patagonian Igneous Metamorphic Belt (CPIMB). The objective of this paper is
29 to better understand the geodynamic and tectonic processes that generated its rocks
30 and structures. More specifically, explanations are offered for different questions: 1) the
31 aforementioned belt corresponds to a collisional or accretionary orogen? 2) during
32 which geological event it was built? 3) how was the South American plate drifting
33 during that process? 4) why the foliation of the rocks of one of its localities presents a
34 different structural attitude than others? To answer these questions, paleogeographic
35 reconstructions were performed based on paleomagnetic data ranging from ca.415 Ma
36 to ca.305 Ma. Through these reconstructions and considering the middle and upper
37 Paleozoic rocks located in a central area of this deformational belt (the Taquetrén
38 range) and the geological background of several authors, it was possible to separate
39 the processes involved in two tectonic cycles: the Chanic (late Devonian) and the
40 Gondwanan (Carboniferous-Permian) events. The CPIMB presents rocks from an
41 ancient orogen that was built mainly during the Chanic event. In the Taquetrén range
42 the orogenic process would extend between approximately 400 Ma and about 360 Ma.
43 Based on the data of this area, the Chanic orogen collapsed between about 360 Ma
44 and about 330 Ma as the result of an abrupt change in the movement of South America
45 along with all the other continents that constituted Gondwana. From a global
46 geodynamic perspective, it is known that Pangea formed on a mantle super-
47 downwelling, where subduction zones surrounded this supercontinent. This caused
48 magmatic processes in its margins and, in the Taquetrén range, triggered a plutonic
49 emplacement in the old structures of the previous metamorphic rocks of the orogen at

50 **Non-peer reviewed EarthArXiv preprint**

51

52 about 315 Ma. In these plutonic rocks, a Gondwanan tectonic event is recorded at
53 about 300 Ma. During this event, a suggested transpressive deformation could have
54 determined the assembly of southern Patagonia with the rest of the lithospheric
55 domains of South America. This tectonic event ended in the central area of CPIMB
56 before the intrusion of non-deformed batholiths during the Permian. **Key words:**
57 Patagonia, orogeny, Chanic event, Gondwanic event, transpressive deformation.

58

59 **1. Introduction**

60 The presence of a middle-late Paleozoic internal deformation zone within Patagonia
61 has been the subject of study for many authors and it has been interpreted in different
62 tectonic scenarios (Forsythe, 1982; Pankhurst, et al., 2006; Ramos, 2008; Varela et al.,
63 2015; Calderón et al., 2016; Suarez et al., 2019; Oriolo et al., 2019; García -
64 Sansegundo et al., 2019; Renda et al., 2019; Renda et al., 2021; Rojo et al., 2021). It
65 belongs to an igneous metamorphic belt in the southern margin of the North
66 Patagonian Massif (NPM, Fig. 1) with a NW-SE trend and its tectonic structures have
67 had a strong influence on the geological evolution of central Patagonia (Figari et al.,
68 2015; Bilmes et al., 2013; Echaurren et al., 2016; Zaffarana et al., 2017; Bucher et al.,
69 2019; Renda et al., 2019; Suarez et al., 2019; Ruiz González et al., 2020; Foix et al.,
70 2020; Giacosa et al., 2020; Serra-Varela et al., 2020; Marcos et al., 2020).

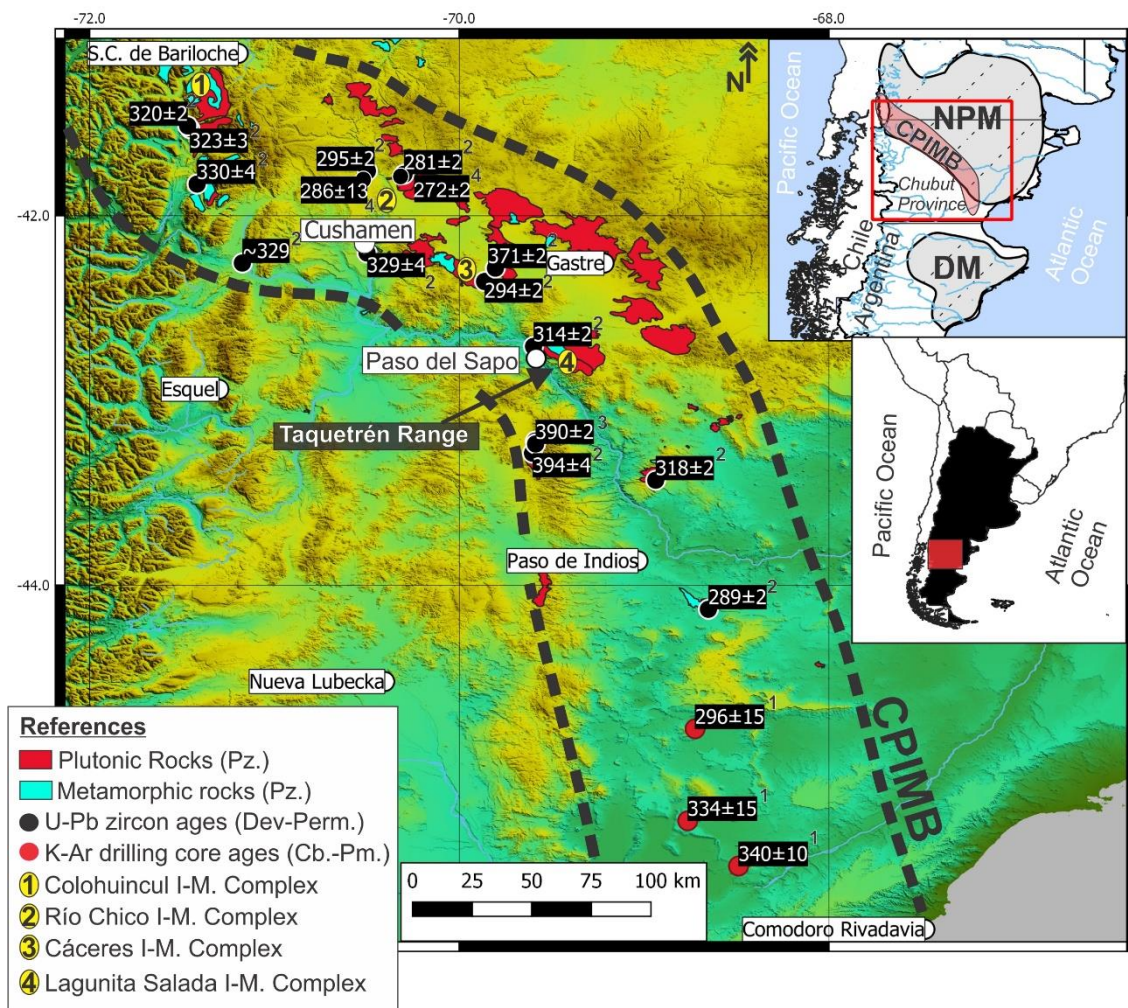
71

72

73

74 Non-peer reviewed EarthArXiv preprint

75



76

77 **Fig.1. Geographic location of the Central Patagonia Igneous Metamorphic Belt**

78 **(based on Renda et al., 2021). The relative geographical location of Taquetrén**

79 **range and Paso del Sapo locality are indicated. Igneous metamorphic (I-M.)**

80 **complexes mentioned in the text, are also shown. NPM: North Patagonian**

81 **Massif. DM: Deseado Massif. CPIMB: Central Patagonian Igneous Metamorphic**

82 **Belt.**

83 The metamorphic and plutonic rocks comprising this belt have been grouped, in

84 general, under the medium-high metamorphic grade Cushmanen Formation

85 (Volkheimer, 1964) and the plutonic Mamil Choique Formation (Ravazzoli and Sesana,

86 **Non-peer reviewed EarthArXiv preprint**

87

88 1977). In some of its specific sectors similar igneous-metamorphic rocks (Fig. 1) have
89 been grouped as Río Chico Complex (Dalla Salda et al., 1994; Cerredo and López de
90 Luchi, 1998; López de Luchi and Cerredo, 2008), Cáceres Complex (Giacosa, et al.,
91 2014) and Colohuincul Complex (Dalla Salda et al., 1991; García Sansegundo, 2009;
92 Oriolo et al., 2019).

93 The metamorphic rocks of Río Chico Complex (Fig. 1) have NW-SE foliations (Dalla
94 Salda et al., 1994) and are intruded by granitoids with ages of 329 ± 4 Ma (U-Pb zircon
95 dating), 286 ± 13 Ma (U-Pb zircon dating) and 295 ± 2 Ma (U-Pb zircon dating) ages
96 (Pankhurst et al., 2006; Varela et al., 2005). The Cáceres Complex (Fig.1) includes
97 high-grade schists, paragneisses, minor amphibolites and orthogneisses (Giacosa et
98 al., 2014). In this complex, the rocks exhibit a main metamorphic foliation striking NNE-
99 SSW and are associated with syntectonic mylonitic granites that yield a 371 ± 2 Ma (U-
100 Pb zircon dating) crystallization age (Pankhurst et al., 2006). These rocks are intruded
101 by post-tectonic granites with a 294 ± 2 Ma (U-Pb zircon dating) age (Pankhurst et al.,
102 2006; Giacosa et al., 2014). Colohuincul Complex (Dalla Salda et al., 1991) is
103 composed by schists, metaquartzites, gneisses, migmatites, foliated amphibolites and
104 amphibolitic orthogneisses, that are intruded by a suite of deformed granitoids. Garnet
105 micaschists have yielded two nearly identical late Pennsylvanian ages of 299 ± 8 Ma
106 and 302 ± 16 Ma (Th+U monazites datings), respectively (Oriolo et al. 2019).

107 It is noteworthy that Varela et al. (2015), working in the northern sector of the CPIMB,
108 pointed out that there are two different Devonian and Carboniferous-Permian igneous-
109 metamorphic events in the CPIMB. These authors distinguished them based on the
110 geochemical differentiation of both episodes that named: Chanic event and
111 Gondwanan event.

112 **Non-peer reviewed EarthArXiv preprint**

113

114 On the other hand, several works have regarded the CPIMB as a Paleozoic orogenic
115 belt (Pankhurst et al., 2006; Ramos, 2008; Varela et al., 2015; Oriolo et al., 2019;
116 Renda et al., 2019; Renda et al. 2021; Serra-Varela et al., 2021). From the western
117 edge of the North Patagonian Massif to the Pacific coast, a Devonian accretionary
118 orogen associated with the accretion of the Chaitenia Island Arc, have been proposed
119 by different authors (Hervé et al., 2016, 2018; Rapela et al., 2021)

120 A recent study of rocks of this basement in the Taquetrén range (Renda et al., 2021),
121 (Fig.1) has also described rocks that were included in the so called Central Patagonian
122 Igneous Metamorphic Belt (CPIMB) and its three complexes are considered as
123 references to perform a geodynamic-tectonic analysis in this paper.

124 The rocks of these complexes are outcropping in the aforementioned range close to
125 the Paso del Sapo locality (42° 44´S, 69° 36´W) in the left margin of the Chubut River
126 (Fig. 1). The oldest has been denominated Lagunita Salada Igneous-Metamorphic
127 Complex (LSIMC, Renda et al., 2021) and comprises gneisses, schists, amphibolites
128 and migmatites, which share a penetrative foliation with a mean orientation of 300°–
129 330°/40°–60°. Based on mineral paragenesis, metamorphic conditions of these rocks
130 are the result of Barrovian-type metamorphism, in upper amphibolite-granulite
131 metamorphic facies (Renda et al., 2021). The electron probe micro-analyzer (EPMA)
132 Th–U–Pb ages of monazites show two main isochron populations at 379 ± 5 Ma and
133 323 ± 5 Ma. This complex is intruded by concordant tonalites, granodiorites, minor
134 pegmatites and felsic dikes, which are grouped in the Paso del Sapo Plutonic Complex
135 (PSPC, Renda et al., 2021). This younger complex has a pervasive foliation N300° -
136 330°/ 50° caused by processes ranging from magmatic flow to solid-state deformation
137 indicating a syntectonic emplacement (Renda et al., 2021). The syntectonic stage is
138 recognized by several microstructures in different minerals (Renda et al., 2021).

139 **Non-peer reviewed EarthArXiv preprint**

140

141 However, PSPC rocks are not affected by the metamorphic conditions that provoked
142 the upper amphibolite-granulite metamorphic facies in LSIMC rocks.

143 Centimeter-to meter-sized metamorphic xenoliths of paragneisses from the LSIMC are
144 common within the granodiorites of PSPC (Renda et al, 2021). A porphyroid granite
145 with marked mylonitic foliation that is found within this plutonic complex, also present
146 subhorizontal lineations with left and right kinematic indicators that can be associated
147 with the presence of a transpressive regime at the time of its emplacements (Renda,
148 2020).

149 An age of 314 ± 2 Ma (Sm-Nd isotopic data) of one granodiorite of this complex has
150 been reported by Pankhurst et al. (2006). Zircon U–Pb analysis by LA-ICP-MS carried
151 out by Renda et al. (2021) in the PSPC shows two distinguishable groups with
152 concordia ages of 314.1 ± 2.2 Ma and 302.8 ± 2.2 Ma obtained in a mylonitic tonalite,
153 interpreted, respectively, as the crystallization and subsequent deformation ages.

154 Both LSIMC and PSPC are intruded by unfoliated granitoids grouped in the Sierra de
155 Taquetrén Plutonic Complex (STPC, Renda et al., 2021). Outcrops are typically
156 rounded landforms of undeformed, granodiorites and granites intruding the LSIMC with
157 sharp and discordant contacts. Renda et al. (2021) suggested a probably late Permian
158 age for this complex, considering other non-foliated leucocratic granitoids outcropping
159 in the area with Cisuralian age (e.g., Laguna del Toro granodiorite, La Potranca
160 granite, see Pankhurst et al., 2006). STPC is considered by Renda et al. (2021) as
161 representative of a post-tectonic magmatism.

162 It is likely that there was a middle to upper Paleozoic orogen crossing Patagonia,
163 however, several questions are still without reasonable answers: 1) Does the Central
164 Patagonian Igneous Magmatic Belt belong to an accretionary orogen or to a collisional
165 one? 2) When was this orogen generated, during the Chanic event or the Gondwanan

166 **Non-peer reviewed EarthArXiv preprint**

167

168 event or both? 3) How was the South American Plate drift when this orogen was
169 formed? 4) Why does the metamorphic foliation of the Cáceres Complex have a
170 different orientation (NNE-SSW) from that of the Río Chico and Lagunita Salada
171 complexes (NW-SE)?

172 On the other hand, a compilation of previously published magmatic and metamorphic
173 ages reveals that, at least, two different Paleozoic magmatic episodes are present in
174 Central Patagonia (Renda et al. 2021). The older is related to medium- high-grade
175 barrovian metamorphism and associated migmatites and igneous rocks with ages from
176 ~400 to 360 Ma and the younger to plutonic rocks with ages spanning from ~330 to
177 270 Ma. There is a magmatic gap of about 30 My between these two episodes
178 (between 360 and 330 Ma), in which amphibolite-granulite metamorphic facies
179 metamorphism was recorded in different sectors of the CPIMB (Renda et al. 2021).
180 Therefore, a model to explain this belt should consider what was the cause of the
181 magmatic lull between the two episodes (Renda et al. 2021).

182 The objective of this work is to answer the questions mentioned above as well as to
183 explain the cause of the magmatic lull of about 30 My between both magmatic
184 episodes.

185 To answer the questions and address the concerns raised above, paleogeographic
186 reconstructions were made using paleomagnetic poles covering a period that extends
187 from approximately 415 Ma to approximately 305 Ma (Table 1). It is noteworthy that
188 from 320 Ma there are models of paleogeographic reconstructions that have been used
189 by Vizán et al. (2015; 2017) to explain different Gondwanan tectonic events. They are
190 the continuation of the processes that are analyzed in this work.

191

192

193 **Non-peer reviewed EarthArXiv preprint**

194

195 **2. Paleogeographic reconstructions**

196 **2.1 Selection of paleomagnetic poles**

197 To perform the reconstructions, paleomagnetic poles (PPs) from continents that made
198 up Gondwana were selected. To analyze the cause of the rapid movement of this
199 mega continent to form Pangea during a period between ca. 360 Ma and ca. 330 Ma,
200 PPs from Europe and North America (continents that formed Laurasia) were also
201 selected.

202

203 **2.2 Selection of Gondwanan Paleomagnetic Poles**

204 In Table 1 there are 27 PPs selected from different crustal blocks that made up
205 Gondwana. The selection was based on the previous ones carried out by McElhinny et
206 al. (2003), Geuna et al. (2008) and Torsvik et al. (2012). All PPs have quality factors Q
207 ≥ 3 with a maximum Q of 7 (Van der Voo, 1993).

208

209

210

211

212

213

214

215

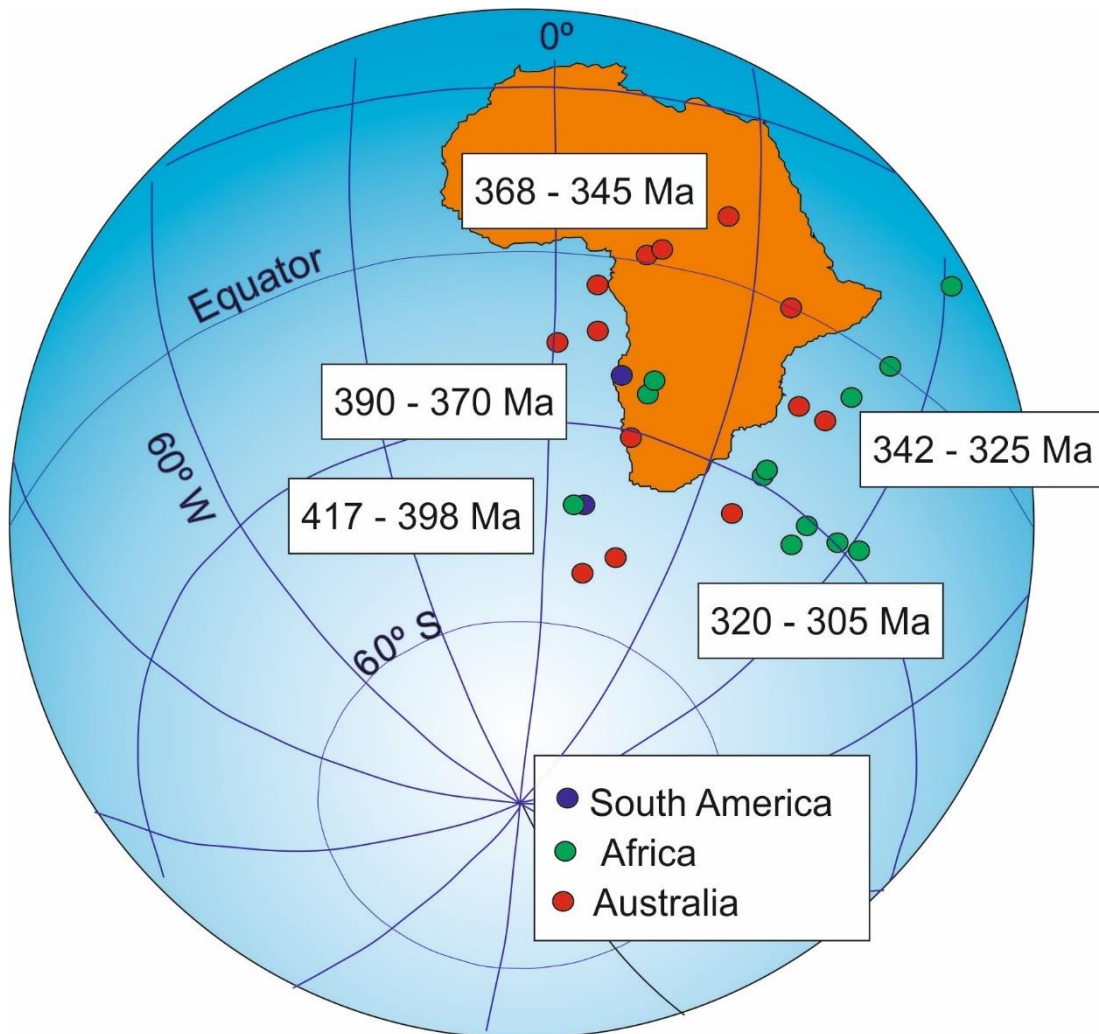
216

217

218

219 Non-peer reviewed EarthArXiv preprint

220



221

222

223 **Fig. 2. Selected paleomagnetic poles of the Gondwanan continents**
 224 **reconstructed in present geographic coordinates of Africa. Age ranges based on**
 225 **those of the selected paleomagnetic poles (Table 1).**

226

227 **2.3 Selection of Laurasian paleomagnetic poles for ca. 360 Ma and ca. 330 Ma**

228 There is a lack of data from Laurasia precisely for a key period (between ca. 360 Ma
 229 and 340 Ma) in which Gondwana, abruptly changed its movement and drifted to the
 230 north to make up Pangea.

231 **Non-peer reviewed EarthArXiv preprint**

232

233 To carry out our analysis, 360 Ma and 350 Ma PPs of the Laurasia spherical spline
234 path of Torsvik et al. (2012) were selected. To obtain a mean paleomagnetic pole for
235 ca. 330 Ma, three PPs from the North American Plate (see Table 2) and two from the
236 United Kingdom were selected.

237

238 **2.4 Paleomagnetic reconstructions**

239 **2.4.1 Reconstruction of Gondwana and South America**

240

241 To perform the reconstruction of Gondwana and South America, it was considered that
242 if the relative positions of several continents are well-known, all being defined in the
243 same plate circuit, the PPs from these continents can be averaged or combined into an
244 apparent polar wander (APW) path (e.g., Besse and Courtillot, 2002). In other words, it
245 is well known that Gondwana was a mega-continent composed by different plates that
246 in the Paleozoic moved together, if an APW path is built for Gondwana with paleopoles
247 of its different continents, the drift of each of them (e.g., South America) can be
248 determined. Selected PPs of different Gondwanan domains were then transferred to
249 the present geographic coordinates of Africa (Fig. 2) using the reconstruction
250 parameters (Euler's poles) of Lawver and Scotese (1987). Africa was chosen as the
251 reference continent to analyze these PPs, since this continent has remained quasi-
252 stationary with respect to longitude throughout Phanerozoic time according to Torsvik
253 et al. (2012) among others. Therefore, other continents, partnered in the same plate
254 circuit, will occupy their own paleolongitudinal positions during successive
255 paleogeographic reconstructions. This is known as the "zero-longitude Africa method"
256 to analyze the movements of Gondwana which is independent of any changes
257 occurring in the mantle as opposed to the "plume generation zone method" which

258 **Non-peer reviewed EarthArXiv preprint**

259

260 requires that the deeper mantle remains stable (e.g., Torsvik et al., 2012). For the
261 analysis of this work, it was considered that the Lawver and Scotese (1987) proposal is
262 a reasonable approximation to Gondwana configuration since it is based on 3
263 arguments: the best fit that can be made between continental platforms (whose limits
264 were defined by geophysical data), the best grouping between paleomagnetic poles of
265 different continents for a given geological time, a properly matching of geological and
266 tectonic features between continents that were contiguous prior to the opening of the
267 Atlantic and Indian oceans.

268 Fig. 2 shows that after the reconstruction of PPs to present Africa geographic
269 coordinates, there are certain trends in the distribution of them. To the west there is a
270 sequence of PPs showing a younger direction to the north. There is another distribution
271 of poles to the east, with the oldest further north than the youngest in the south.
272 As mentioned above, to analyze the drift history of a continent, a sequence of PPs are
273 combined in APW paths and there are different ways to set up them, a recognized and
274 widely used method is the running mean path (e.g., McElhinny et al., 2003; Torsvik et
275 al. 2012). If this method is used for the selected PPs, the Fisher (1953)'s statistical
276 parameters indicate low precision for the calculated mean PPs (with 95% interval of
277 confidence, A_{95} , greater than 15° and precision parameter, Kappa (K), less than 10).
278 Therefore, it was preferred to average PPs that were geographically grouped and that
279 corresponded to limited time periods as Van der Voo (1993). Certain control criteria
280 were considered to determine the averages of the selected PPs. Van der Voo (1993)
281 showed that the mean of at least 4 data is robust enough to determine the
282 "paleomagnetic" spin axis of the Earth. Therefore, the number of data that was
283 averaged in each time period was equal to or greater than four and the calculated five

284 Non-peer reviewed EarthArXiv preprint

285

286 mean PPs show K values of 123.98, 83.98, 45.83, 34.13, and 75.32 with respectively
287 A_{95} of 8.3°, 8.4°, 11.4°, 11.6° and 7.0° (Table 3, Fig. 3). These mean PPs are reliable
288 enough for tectonic/geodynamic models and their geographic distribution is somewhat
289 similar to that of the mean PPs from the APW path of McElhinny et al. (2003).
290 Paleomagnetic poles found in databases correspond to works in which their ages were
291 determined through different studies that could be outdated. They correspond to
292 different radiometric dating methods or based on stratigraphic or paleontological
293 analyses. A check was made with an updated compilation of paleomagnetic data
294 (Geuna, personal communication) in order to recognize if there were new ages for the
295 rocks from which the PPs came from. No appreciable differences were recognized with
296 those considered in Table 1. Then, to assign ages to the calculated mean PPs, a
297 transient compromise was adopted and the arithmetic average of all the ages involved
298 in each period and the average between the age of the oldest and the youngest PP of
299 every time, were considered as possible ages (Fig. 3).

300

301

302

303

304

305

306

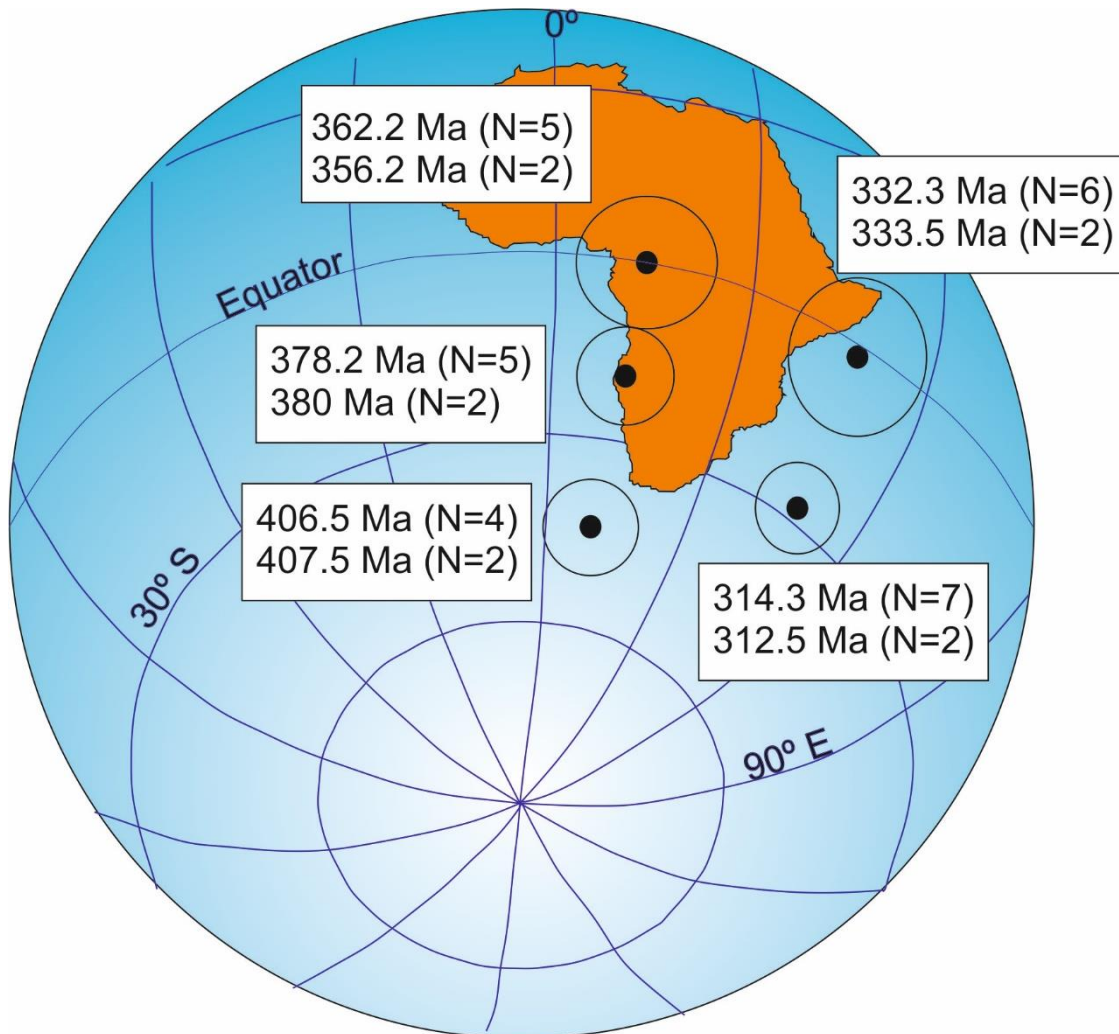
307

308

309

310 Non-peer reviewed EarthArXiv preprint

311



312

313

314 **Fig. 3. Mean paleomagnetic poles of Gondwana and their assigned ages (see text**

315 **for further explanation).**

316

317

318

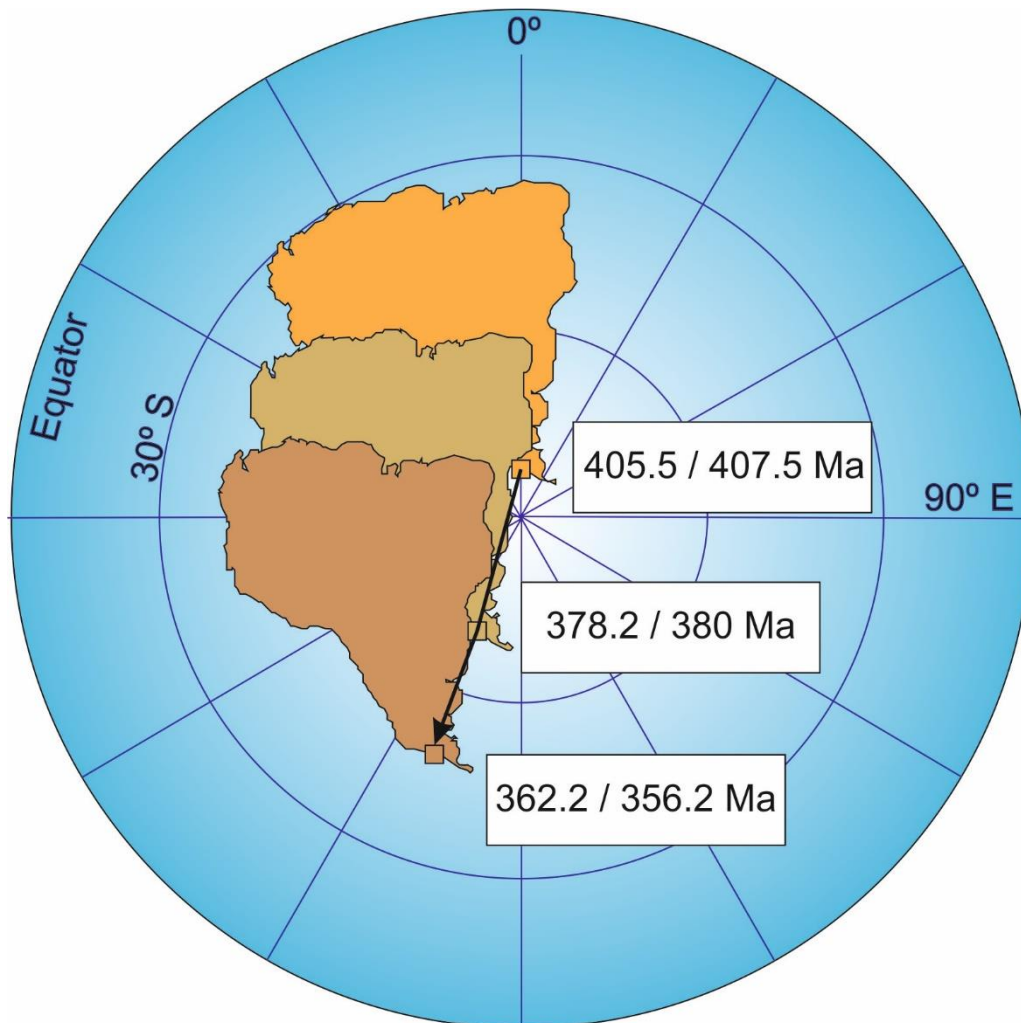
319

320

321

322 Non-peer reviewed EarthArXiv preprint

323



324

325 **Fig. 4. Paleogeographic reconstructions of South America (Euler's poles in Table**
 326 **5) determined with Gondwana paleomagnetic poles. Squares: relative**
 327 **geographic locations of the Taquetrén range at different times. Black arrow:**
 328 **displacement vector for this range for a time span between about 405 Ma and**
 329 **about 360 Ma.**

330

331 With these average PPs, the Euler's poles were calculated to perform paleogeographic
 332 reconstructions of Africa (Gondwana) and South America (Tables 4 and 5).

333

334 **Non-peer reviewed EarthArXiv preprint**

335

336 Figures 4 and 5 show successive paleogeographic reconstructions of South America.

337 According to the papers cited in Section 1, it was considered as a working hypothesis

338 that the Central Patagonia Igneous Metamorphic Belt (CPIMB), which includes the

339 Taquetrén range (Fig.1), was practically the limit between the continental lithosphere of

340 Gondwana and the oceanic lithosphere of Panthalassa (the old Pacific Ocean).

341 Therefore, using several localities of this belt, the old geographical location of the

342 southern limit of the South America platform was determined. In Figs. 4 and 5,

343 Taquetrén range (see Fig. 1 for the present location) is located according to the

344 geographic coordinates that correspond to it in each time. Southern Patagonia, with the

345 Deseado Massif, would constitute a peri-Antarctic block that was accreted to South

346 America during the Permian due to a toroidal plate motion (Vizán et al., 2015, 2017).

347 It is noteworthy that for the late Paleozoic there was a relevant tectonic activity in

348 southwestern Gondwana related to the accretion of different blocks (e.g., Hervé et al.,

349 2016; 2018; Calderón et al. 2016; Suarez et al., 2019; 2021). Rojo et al. (2021) have

350 hypothesized that the northern portion of the Antarctic Peninsula accreted to the

351 southern margin of Deseado Massif during the mid-Carboniferous.

352

353

354

355

356

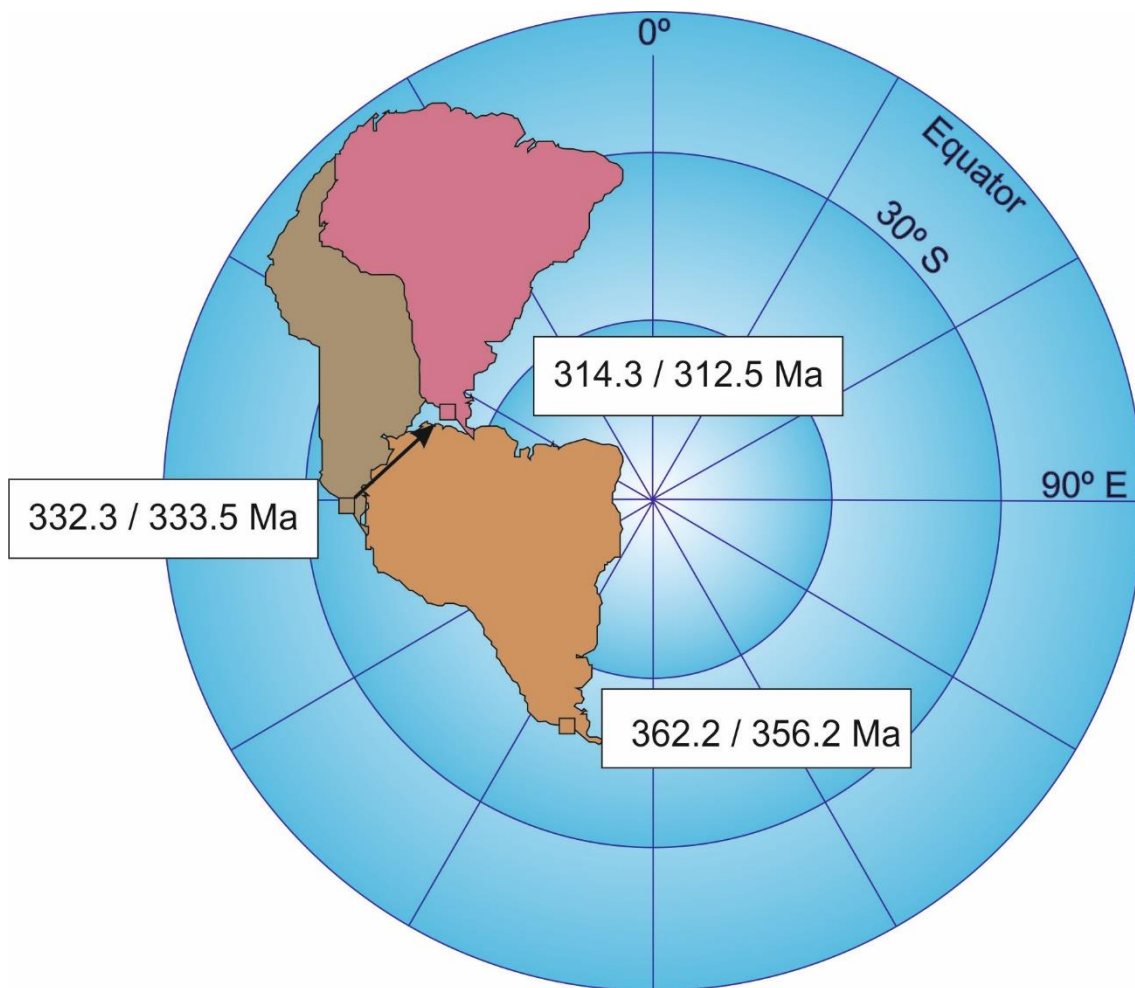
357

358

359

360 Non-peer reviewed EarthArXiv preprint

361



362

363

364 **Fig. 5. Paleogeographic reconstructions of South America determined with**
 365 **Gondwana paleomagnetic poles (Euler´s poles in Table 5). Squares: relative**
 366 **geographic locations of the Taquetrén range at different times between about**
 367 **360 Ma and about 314 Ma. Black arrow: displacement vector for Taquetrén range**
 368 **for a time span between about 330 Ma and about 314 Ma.**

369

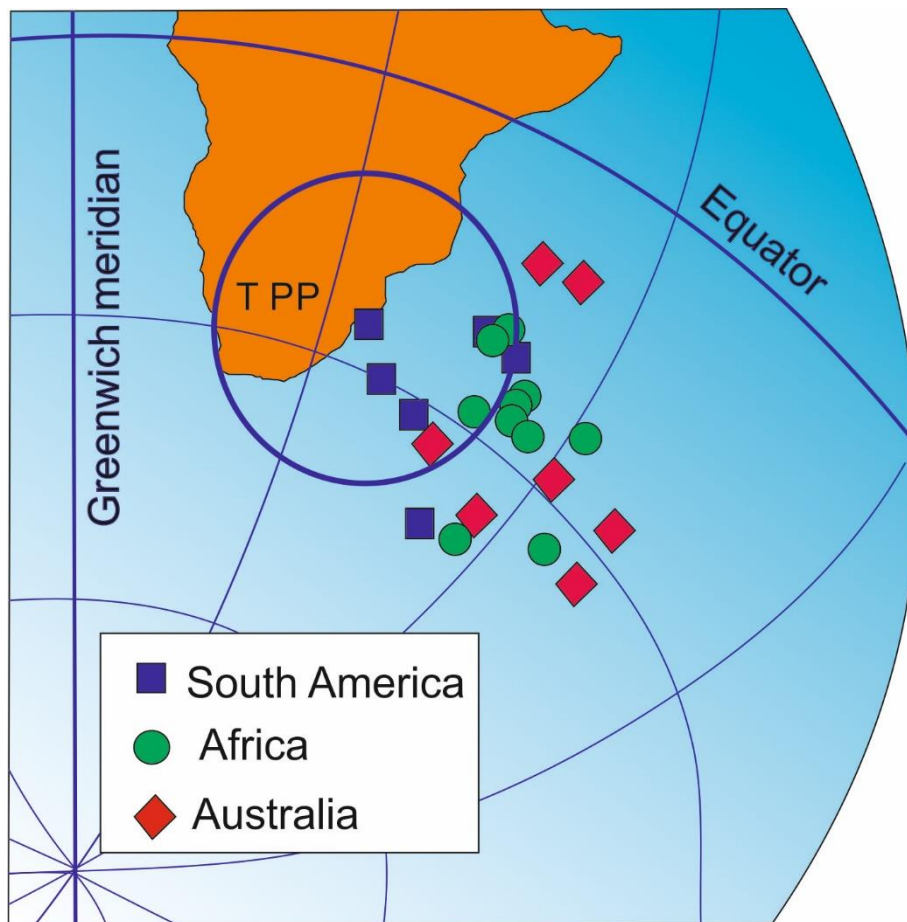
370

371

372

373 Non-peer reviewed EarthArXiv preprint

374



375

376

377 **Fig. 6. late Carboniferous-early Permian poles of Gondwana in present African**
 378 **geographic coordinates. TPP: Paleomagnetic pole of the Tepuel Group with its**
 379 **95% confidence interval.**

380

381 To locate southern Patagonia in Gondwana reconstructions, it was considered again
 382 that this block was a peri-Antarctic block, but a different paleomagnetic reconstruction
 383 was obtained with respect to that of Vizán et al. (2015, 2017). Taking the PP selected
 384 by Vizán et al. (2015, their table 1), a fit of the PP of the Tepuel Group (Rapalini et al.,
 385 1994) was improved with the late Carboniferous ages of Gondwana, mainly with those
 386

387 **Non-peer reviewed EarthArXiv preprint**

388

389 of South America. (Fig. 6). Euler's pole to place southern Patagonia at the present
390 geographic coordinates of Africa in the Gondwana reconstruction has the following
391 coordinates and angle of rotation: Lat.= 34.64° N, Lon.= 18.59° O,
392 Ang.(counterclockwise)= 74.98°. In addition, there are 2 different arguments that
393 support a reconstruction of southern Patagonia as a peri-Antarctic block during the late
394 Paleozoic. 1) The southern Patagonian block involves the Tepuel-Geona basin and
395 further south, the Deseado Massif (e.g., Taboada et al., 2016). Paleobiogeographic
396 studies by Taboada and Shi (2011) indicate that the Tepuel-Genoa basin would have
397 been located at high latitudes (approximately 70°) between the middle Carboniferous
398 and the earliest Permian. This is the paleolatitude that corresponds to the center of this
399 basin in a reconstruction of that age with southern Patagonia as a peri-Antarctic block.
400 2) Through Re-Os dates of southern Patagonia, Mundl et al. (2015) connect the
401 Deseado Massif with the Precambrian Namaqua-Natal belt of South Africa (Eglington,
402 2006). Meanwhile, Precambrian xenoliths from Pali Aike-Tres Lagos (extreme south of
403 Santa Cruz Province) according to Mundl et al. (2015) are connected with the
404 Shackleton range. Precambrian xenoliths of northern Patagonia that belong to the
405 lithospheric subcontinental mantle (LSM), were significantly affected by metasomatic
406 processes and they were not use to make any connection with other localities of
407 Gondwana (Mundl et al. 2016).
408 On the other hand, Schilling et al. (2008) based on Re-Os isotope constraints,
409 proposed that Deseado Massif was probably not far from Malvinas/Falkland Islands
410 since the time of the Proterozoic supercontinent of Rodinia.

411

412

413 **Non-peer reviewed EarthArXiv preprint**

414

415 **2.4.2 Reconstructions of Gondwana and Laurasia before and after the assembly**
416 **of Pangea**

417

418 For more than 40 years, it has been discussed how was the late Paleozoic
419 configuration of Pangea when it was formed, based on paleomagnetic data. There are
420 authors that support a model similar to Wegener's, called Pangea A (e.g., Van der Voo
421 and French, 1974; 1976; Scotese, 2001; Domeier et al., 2012; Pastor Galán, 2022)
422 while others consider a different configuration in which the present southeastern coast
423 of North America would be attached to the northwestern coast of South America
424 according to a model called Pangea B (e.g., Irving, 1977, Morel and Irving, 1981,
425 Muttoni et al. 2003, Gallo et al. 2017). All these authors share the idea that the
426 configuration of Pangea proposed by Wegener corresponds to the Jurassic just before
427 the break- up of this supercontinent and the origin of the Atlantic Ocean.

428 The problem that has generated the difference between configurations of Pangea when
429 assembling, arise from paleomagnetic databases. For a period that extends between
430 the Carboniferous and the Triassic, these databases may present several PPs that
431 could correspond to remagnetizations (see discussion of Domeier et al., 2012) or to
432 paleomagnetic data with insufficient tectonic corrections due to undetected vertical axis
433 tectonic rotations of sampled cortical blocks (Pastor Galán, 2022).

434 For Hallam (1982), the best approach to evaluate the models of Pangea A and B is to
435 use geological/structural data. For example, for a model of Pangea B (with the best fit
436 of late Carboniferous PPs) to evolve into one of Pangea A (valid for the Jurassic), a
437 huge shear zone involving a lateral displacement of at least 3,500 km between
438 Laurasia and Gondwana is required. No strong geological evidence has been found to
439 justify this shear zone supporting the evolution from a model of Pangea B to one of

440 Non-peer reviewed EarthArXiv preprint

441

442 Pangea A. Weil et al. (2001) demonstrated that the Cantabria-Asturias arc underwent
443 true (100%) oroclinal bending during Pennsylvanian and Permian times of an originally
444 linear belt, and this tectonic scenario does not support a 3,500 km dextral megashear
445 to evolve from one model of Pangea B to another of Pangea A. According to Hopper et
446 al. (2017) the collision to form Pangea involved an overthrust from Gondwana to
447 Laurentia causing a crustal shortening of more than 300 km, and this process excludes
448 any possibility of a lateral displacement of about 3,500 km.

449 Therefore, to perform the paleogeographic reconstructions for 362.2/356.2 Ma and
450 333.5/332.3 Ma, it was considered that Pangea was formed according to a model
451 similar to that proposed by Wegener (called Pangea A).

452 To carry out the global paleogeographic reconstruction for 362.2 / 356.5 Ma (Fig. 7a),
453 Gondwana was located considering that Africa had negligible longitudinal
454 displacements and using the paleomagnetic pole calculated for the corresponding
455 period. Table 4 shows the Euler's pole to carry out this reconstruction. To reconstruct
456 Laurasia, the 360 and 350 Ma paleopoles calculated by Torvisk et al. (2012, their Table
457 5) were averaged and this mean was brought to coincide with the axis of rotation of the
458 Earth in the southern hemisphere (rotating in this way also Laurasia). This continent
459 was then rotated using a Euler's pole centered at the south geographic pole (latitude
460 90°S) to face the NW coast of Gondwana leaving the Rheic Ocean open (Fig. 7a). The
461 Euler's pole comprising all movements to reconstruct Laurasia was Lat.= 14.12°N,
462 Lon.= 45° E, Ang. (counterclockwise) = 75.52°.

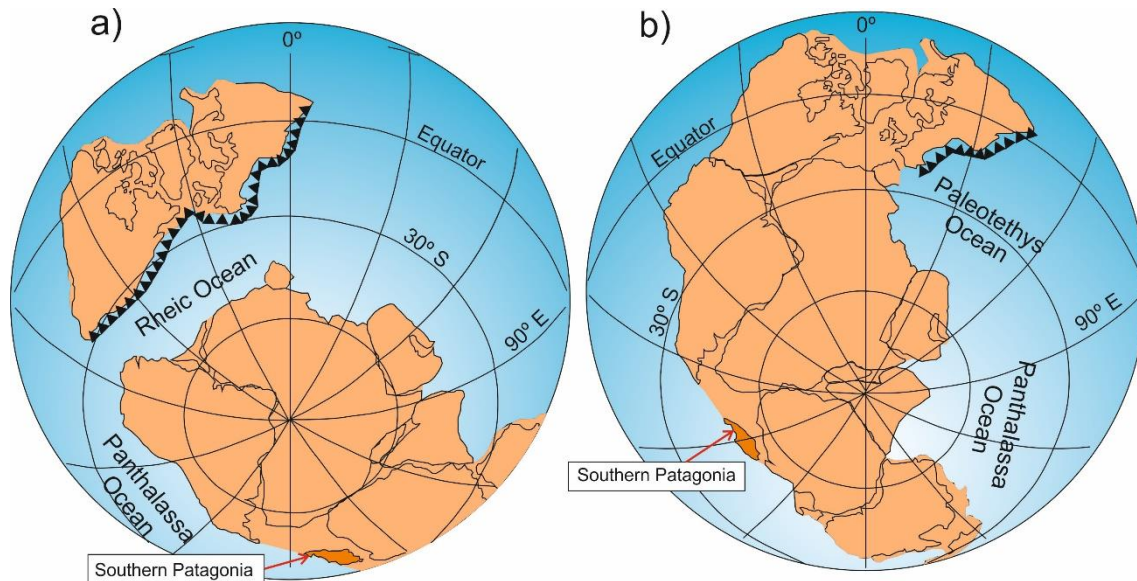
463

464

465

466 Non-peer reviewed EarthArXiv preprint

467



468

469

470 **Fig. 7. Paleogeographic reconstructions of Gondwana (Euler's poles in Table 4)**
 471 **and Laurasia before and after the formation of Pangea. Notice the position of**
 472 **Southern Patagonia respect to South America. a) Laurasia was reconstructed**
 473 **latitudinally and facing the northwest border of Gondwana as explained in the**
 474 **text. Siberia is not represented because it is attached later to Pangea. b) Pangea**
 475 **was already formed and moving to the NE.**

476

477 It is noteworthy that Pangea started an assembly through a diachronic collision
 478 between Gondwana and Laurasia at ca. 340 Ma (e.g., Nance et al., 2012). In any case,
 479 it is considered that Gondwana was already attached to Laurentia at about 330 Ma
 480 (Pastor Galán, 2022).

481 To perform the paleogeographic reconstruction for 332.3 / 333.5 Ma (Fig. 7b), the PPs
 482 of United Kingdom were transferred to North America Plate using Alvey (2009)'s Euler
 483 pole (Lat.= 78.6° N, Lon.= 161.9° E, Ang. (clockwise rotation)= 31°). In this plate all the
 484

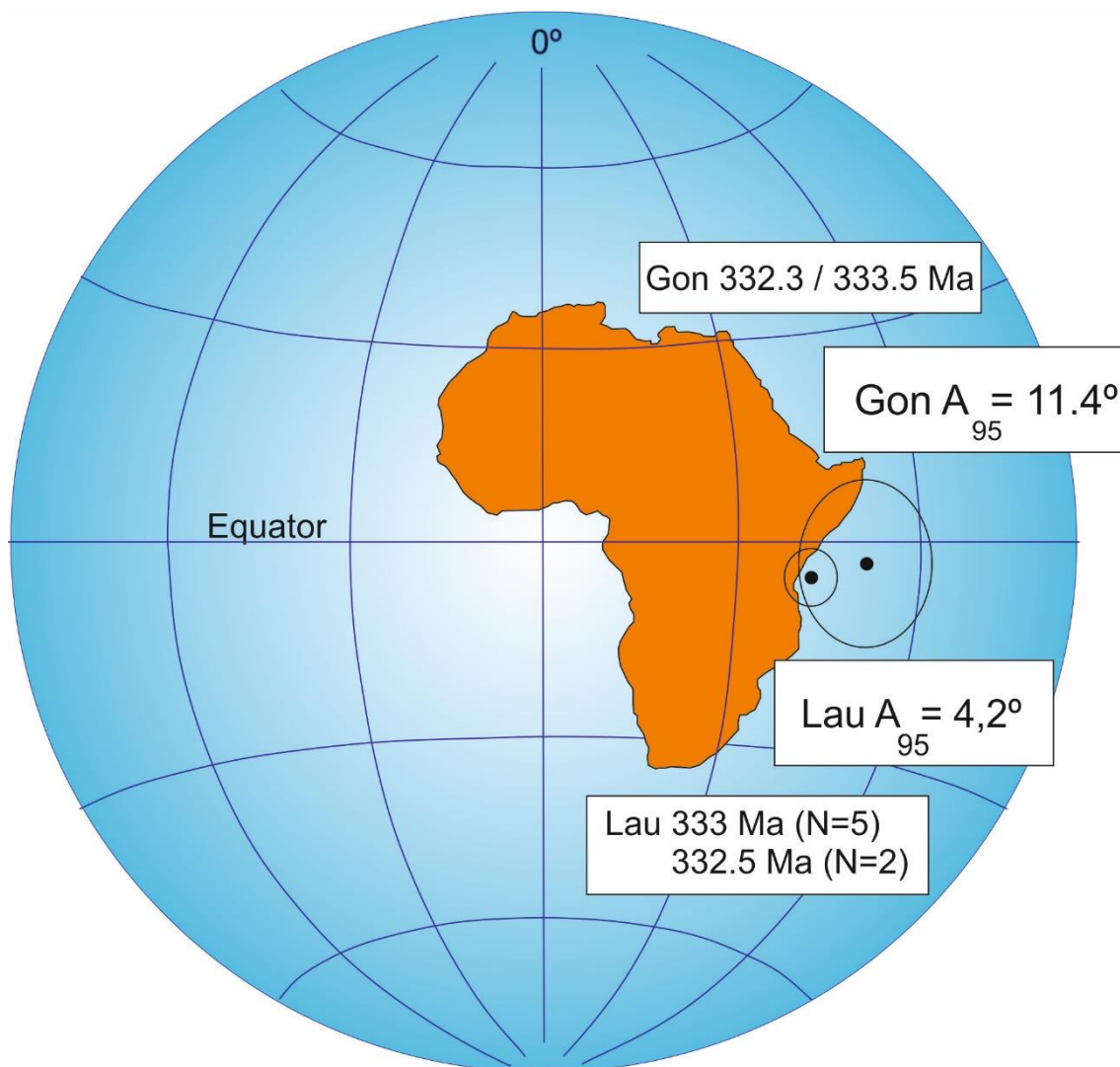
485 **Non-peer reviewed EarthArXiv preprint**

486

487 selected PPs for Laurasia were averaged and the mean was transferred to Africa,
 488 using a Euler's pole as that proposed by Bullard et al. (1965). Then, a
 489 counterclockwise rotation was applied to Laurasia with respect to Gondwana using a
 490 Euler's pole as that of Van der Voo and French (1974) that closes the Gulf of Mexico.
 491 The Euler pole corresponding to both motions of Laurasia is Lat.= 56.7° N, Lon.=
 492 338.3° E, Ang. (counterclockwise) = 92.7°.

493

494



495
 496

497 **Non-peer reviewed EarthArXiv preprint**

498

499 **Fig. 8. Mean paleomagnetic poles (PP) of about 333 Ma of Gondwana (Gon) and**
500 **Laurasia (Lau) with their 95% intervals of confidence (A_{95}) in current Africa**
501 **geographic coordinates. N: number of data used to average the mean age for**
502 **Laurasia PP. N=5 includes the ages of all PPs that were averaged, N=2 mean**
503 **between the youngest and oldest selected PPs.**

504

505 Although it was not possible to obtain an optimal fit between Laurasia and Gondwana
506 PPs for ca. 330 Ma (Fig.8), the mean Laurasian paleopole is included by the
507 confidence interval of the Gondwana pole. Then, it was considered that the
508 reconstruction obtained in this way could belong to a plausible model of Pangea A. It is
509 possible that the lack of better adjustment between PPs of Gondwana and Laurasia is
510 due to different factors among which, as mentioned above, the unrecognized
511 remagnetizations and incomplete structural corrections are the most relevant.

512

513 **3. Global geodynamic context from the movement of Gondwana to form**

514 **Pangea till Pangea break-up**

515

516 To understand the different tectonic processes that occurred in the CPIMB after 360
517 Ma, it is important to analyze them in a global context, since they are linked to the
518 geodynamics of Gondwana and Pangea.

519 The change in the paleogeographic location of South America (and consequently of
520 the Taquetrén range) between 362.2/356.2 Ma and 333.5/332.3 Ma (Fig. 5), would
521 involve two movements of Gondwana (Figs. 7a and 7b). The first movement would
522

523 Non-peer reviewed EarthArXiv preprint

524

525 correspond to the drift of Gondwana pulled by the subduction of Laurasia to closure
526 the Rheic Ocean (Nance et al., 2012). The second movement involves to Pangea
527 drifting to the NE.

528 The movements of Gondwana mentioned above would involve a drift speed that is not
529 observed at Present times in any continent. It is also greater than that which
530 corresponded to India in its drift from Gondwana to Asia possibly due to Neotethys
531 Ocean slab pull. While the speed of India was 17 cm/ year (Kumar et al., 2007), the
532 speed of Gondwana calculated for Taquetrén range using the averages between the
533 extreme age values of each period (356.5 Ma and 333.5 Ma), is 23.77 cm/ year and
534 using the mean of all the ages of the PPs of each period (ages between 362.2 Ma and
535 332.3 Ma) is 18.29 cm/year. To check the obtained velocity values, the same
536 calculation was performed for the Taquetrén range, using the mean PPs of 360 and
537 340 Ma of McElhinny et al. (2003). In this case the value is 22.42 cm/year.

538 The lack of paleomagnetic data with ages close to 350 Ma from the continents that
539 formed Gondwana, could bias the calculations of the speeds mentioned above.

540 However, it is evident, that according to the available data, an abrupt change in the
541 direction of movement of South America (Gondwana) can be recognized after about
542 360 Ma.

543 It is interpreted that Gondwana was pulled by subduction at the northern margin of the
544 Rheic Ocean (Fig. 7a) toward a super-downwelling in the mantle (Zhong et al., 2007; Li
545 and Zhong, 2009) to form Pangea at about 340 Ma. Tectonic processes that occurred
546 in Gondwana from the formation of Pangea to its dismemberment must be analyzed

547

548

549 **Non-peer reviewed EarthArXiv preprint**

550

551 considering the changes that occurred in the terrestrial mantle that caused a global
552 change from contractional to extensional tectonic processes.

553 Different authors have suggested that supercontinents like Pangea form on the surface
554 of the Earth above super-downwellings in the mantle that causes the attraction of all
555 lithospheric fragments that are assembled (Zhong et al., 2007; Maruyama et al., 2007;
556 Santosh et al., 2009; Yoshida and Santosh, 2011).

557 Then, the slab pull in the southern margin of Laurasia could have been incentivized by
558 a super-downwelling, causing the fast speed of Gondwana mentioned above, and then
559 its collision with Laurentia, closing part of Rheic Ocean and leaving Paleotethys Ocean
560 open (Fig. 7a and 7b). This collision would cause a linear momentum transfer from
561 Gondwana to Laurasia and the whole Pangea would begin drifting to the N (Vizán et
562 al., 2017). This movement triggered a process of subduction of oceanic plate under
563 oceanic plate further north in a zone of lithospheric weakness (Sears, 2012),
564 generating island arcs (e.g., Wrangelia and Kolyma super-terrane) accreted, latter, in
565 the northwest coast of Alaska and the north coast of Siberia (Nokleberg, et al. 2001). In
566 turn, on the boreal margin of the Paleotethys Ocean, a process of slab pull gave rise to
567 a Pangea self-subduction processes (Gutiérrez-Alonso et al., 2008). The SW-NE
568 displacement vector between 332.3/ 333.5 Ma and 314.3/ 312.5 Ma (Fig.5) is that
569 determined by Vizán et al. (2015; 2017). It corresponds to both: the northward
570 movement of Pangea and the slab pull of Paleotethys Ocean causing the Pangea self-
571 subduction and a toroidal convection in the sense of Bercovici et al. (2000). It is
572 noteworthy that the intraplate deformation in Gondwana began about 30 My after
573 Pangea formation (e.g., Pastor Galán et al., 2013; Vizán et al., 2017).

574

575 Non-peer reviewed EarthArXiv preprint

576

577 The super-downwelling where it was assembled Pangea caused a global contraction of
578 this supercontinent (Yoshida and Santosh, 2011) that consequently it was surrounded
579 by subduction zones (Zhong et al., 2007; Li and Zhong, 2009).

580 The slabs of the subduction surrounding Pangea in a super-downwelling, would cause
581 tectonic erosion of the continental crust and transport of sediments to deep zones of
582 the mantle (Senshu et al., 2009). In this way, radiogenic elements found in the crust (U,
583 Th, K) would reach the deepest mantle causing, a hot anomaly (Senshu et al. 2009).
584 This anomaly, together with the heat coming from the core would cause the birth of a
585 hot super plume or upwelling (Senshu et al., 2009).

586 On the other hand, the slabs of the subduction zones surrounding Pangea, would
587 penetrate the lower mantle and would drive the return of the hot upwelling from the
588 deepest mantle to the lithosphere (Chase and Sprowl, 1983; Zhong et al., 2007; Zhang
589 et al.,2010). Faccenna et al. (2021) proposed that this whole mantle convection cell
590 was triggered by slab-suctions bordering the margins of Pangea during the late
591 Paleozoic.

592 The thermal shielding caused by the continental lithosphere of Pangea (Anderson,
593 1982; Gurnis, 1988; Coltice et al., 2007), would help further warming of the mantle
594 below. Finally, the hot upwelling would cause intraplate magmatic processes and
595 extensional tectonics and would be a fundamental factor in the break- up of Pangea
596 (Gurnis 1988). For Zhong et al. (2007), about 50 million years should pass between the
597 establishment of the subduction zones surrounding a supercontinent and the beginning
598 of extensional tectonic processes in its crust.

599

600

601 **Non-peer reviewed EarthArXiv preprint**

602

603 **4. Discussion**

604

605 As considered by other authors (e.g., Scotese, 2001), our paleogeographic
606 reconstructions based on paleomagnetic data are interpreted as representative of plate
607 tectonic processes. In this way, movements linked to true polar wander (TPW, the
608 body-solid rotations of the Earth with respect to its spin axis) are not considered.
609 According to Merdith et al. (2021) geology is frequently silent on the positioning of
610 continents, however it contains wealth information of plate motions. For this reason, in
611 this work it was consider the geology in Central Patagonia (e.g., Taquetrén range) as a
612 case study for analyzing the processes occurred in the southwestern margin of
613 Gondwana.

614 To carry out our geodynamic/tectonic interpretations, it was regarded that the
615 displacement vectors for a given locality, when drifting with its continent, may have an
616 orientation similar to that of the tectonic stresses that would act when this locality is
617 deformed (e.g., Reilinger et al., 2006, Vauchez et al., 2012).

618 All tectonic plates on our planet are in motion. However, since only continental plate
619 reconstructions were performed in this work, drift from the Panthalassa Ocean floor is
620 omitted from this analysis and it is considered as a stationary frame of reference.

621 In Figures 4 and 5 successive paleogeographic reconstructions of South America are
622 represented between 407.5/406.5 Ma and 314.3/312.5 Ma.

623 Taquetrén range is also represented in its relative location corresponding to each age.

624 Except for the period between 362.2/356.2 Ma and 333.5/332.3 Ma, the displacement

625

626

627 **Non-peer reviewed EarthArXiv preprint**

628

629 vectors of the mentioned locality are represented between successive paleogeographic
630 reconstructions.

631

632 It is noteworthy that the tectonic interpretations of this paper were made considering for
633 the southern Argentine margin of the North Patagonian Massif what was indicated by
634 von Gosen (2009): the suture suggested between this massif and southern Patagonia
635 (e.g., Ramos, 2008) is not yet restricted by relicts of ophiolites.

636 Through our reconstructions, an analysis can be made at the CPIMB that includes two
637 different tectonic events that are correlatable with the magmatic episodes reported by
638 Renda et al. (2021, their Fig. 12c), and are differentiated by Varela et al. (2015)
639 through geochemical data such as Chanic event and Gondwanan event (see Section
640 1).

641 Among the magmatic episodes reported by Renda et al. (2021) there is a period of
642 magmatic lull that coincides with the movement of South America (Gondwana) to form
643 Pangea (Fig. 7a and 7b).

644

645 **4.1 Chanic event (ca. 400 – 360 Ma) in the CPIMB**

646

647 The three paleogeographic reconstructions between 407.5/406.5 Ma and 362.2/356.2
648 Ma (Fig. 4) indicate a NE - SW movement of South America, with velocities of less than
649 15 cm/ year for the Taquetrén range (Table 6). This differs from what was pointed out
650 by Domeier and Torsvik (2014) who propose that Gondwana remained relatively
651 stationary between 390 Ma and 360 Ma.

652 According to the observed movement of South America, the displacement vector of
653 Taquetrén range (Fig. 4) and the kinematic inferred from the structures of the

654 **Non-peer reviewed EarthArXiv preprint**

655

656 metamorphic rocks of LSIMC (e.g., metamorphic penetrative foliation with a mean
657 orientation of 300° – $330^{\circ}/40^{\circ}$ – 60° , top-to-the-southwest tectonic transport direction
658 according to Renda et al., 2021), it is interpreted that during a period between
659 approximately 400 Ma and 360 Ma, an accretionary orogen as those described by
660 Cawood et al. (2009) was generated (Fig.9a) where the CPIMB is at Present. The
661 same interpretation has been done by Rapela et al. (2021) based on other
662 methodologies.

663 According to the calculated velocities, it is possible that the NE-SW movement of South
664 America could have been relatively fast. Although we do not consider the movement of
665 the oceanic plates of Panthalassa Ocean, a mountain range built during Chanic event,
666 would correspond to an advancing orogen as the Andes (see Royden, 1993 or Cawood
667 et al., 2009) with its associated magmatism. This proposal is in agreement with Serra-
668 Varela et al. (2021) who proposed that an Andean-type subduction related margin has
669 been active in the southwestern of the Gondwana border from the early Devonian up to
670 the early Carboniferous.

671 In other words, it is interpreted that the rocks of LSIMC were affected by a regional
672 compression. These metamorphic rocks are, indeed, typical of areas of mountain belt
673 formation. NW-SE foliation was formed perpendicular to the NE-SW direction of
674 principal stress, recording the direction of shortening of an accretionary orogen
675 (Fig.9a).

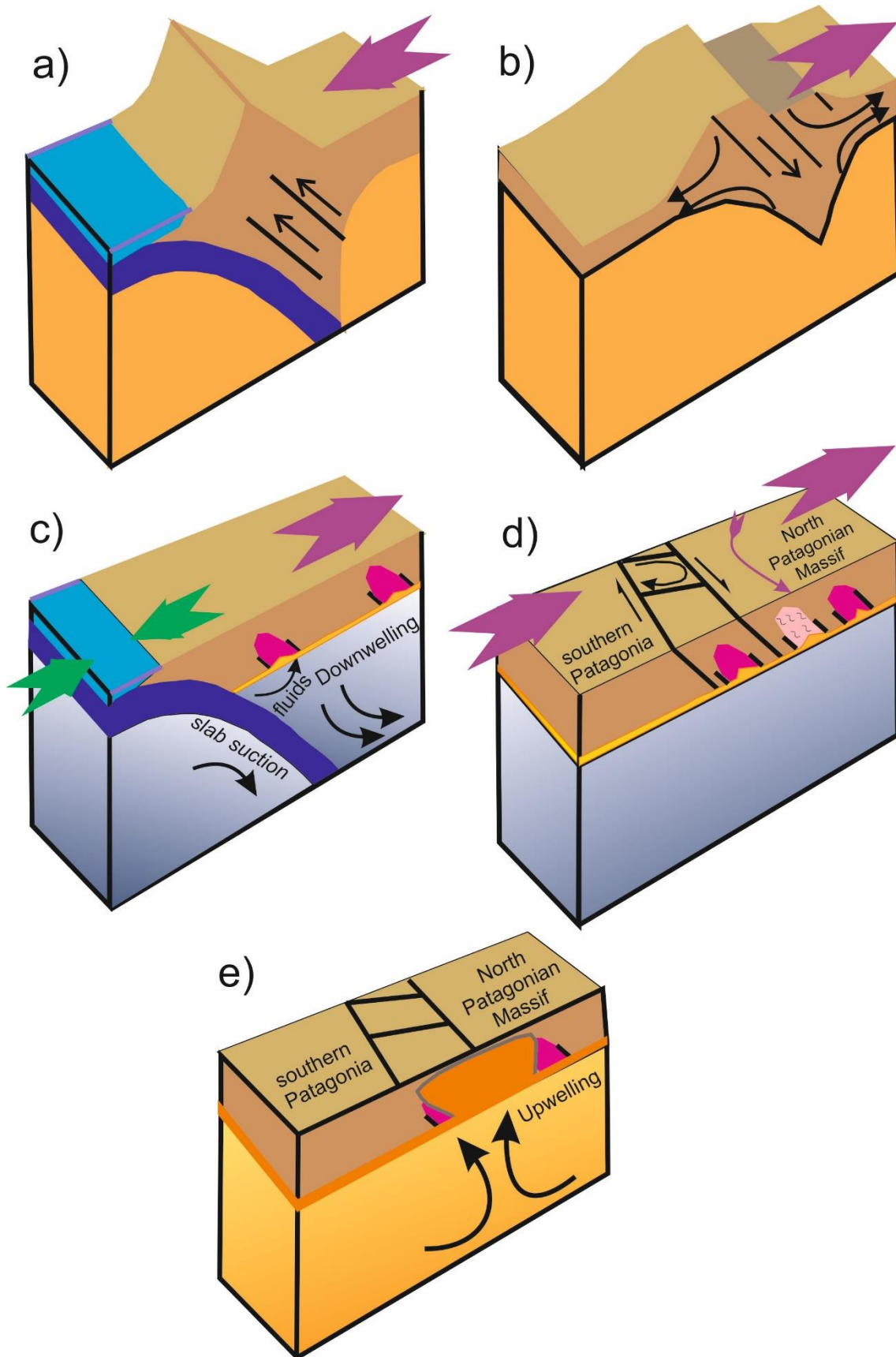
676

677

678

679

680



683 **Non-peer reviewed EarthArXiv preprint**

684

685 **Fig.9. Proposal for the temporal evolution of the geodynamic processes that**
686 **have occurred in the Central Patagonia Igneous Metamorphic Belt through**
687 **simplified diagrams (purple arrows: directions of movements of South**
688 **American continental domains). a) Building of the accretionary orogen between**
689 **ca. 400 Ma and ca. 360 Ma (metamorphic rocks of Lagunita Salada Complex in**
690 **brown). b) Collapse of the orogen located in the southern margin of the North**
691 **Patagonian Massif between ca. 360 Ma and ca. 340 Ma. c) Origin of the plutonic**
692 **rocks of the Paso del Sapo Plutonic Complex (in pink) at approximately 315 Ma,**
693 **arrows in green indicate that the subducting and overriding plates are forced to**
694 **drive symmetrically towards the subduction zone due to slab-suction. d)**
695 **Suggested dextral transpression that attached southern Patagonia with the**
696 **North Patagonian Massif at about 300 Ma. In light pink: mylonite. e) Growth and**
697 **emplacement of the Sierra de Taquetrén Plutonic Complex batholith during the**
698 **Cisuralian (Permian).**

699

700 **4.2 Period of magmatic lull in the CPIMB between ca. 360 Ma and 340 Ma**

701

702 As mentioned in Section 1, according to Renda et al. (2021) there is a magmatic gap of
703 about 20 My (between ca. 360 and ca. 340 Ma) after the Chanic event. During this gap
704 a metamorphic peak of amphibolite-granulite facies was developed at about 350 Ma in
705 different sectors of the CPIMB (Renda et al. 2021). The paleogeographic
706 reconstructions (Figs. 4 and 5) indicate the drastic change in the directions of
707 movement of South America (analyzed before, Section 3) occurred during the
708 magmatic gap. Therefore, it is interpreted that in the margin where the CPIMB is at

709

710 **Non-peer reviewed EarthArXiv preprint**

711

712 Present located, the subduction stopped and the accretionary orogen formed between
713 approximately 400 Ma and 360 Ma at the southern margin of the North Patagonian
714 Massif, collapsed (Fig. 9b) by the drastically changing direction movement of South
715 America. Different processes can cause the extensional collapse of an orogen (Dewey,
716 1988). As reviewed by Rey et al. (2001), one of these processes is the change in plate
717 motion. The conditions of an accretionary orogen are favorable for the development of
718 the free-boundary collapse mode of Rey et al (2001). The former active continental
719 margin acts as a free-boundary providing enough space for the bulk extension of the
720 orogene thickened crust, involving simultaneous upper, middle and lower crustal
721 thinning. This process can exhume the middle crust to the surface generating
722 metamorphic core complexes (Badahori et al., 2022) that are recognized in both
723 collisional-type and Andean-type orogen collapses (e.g., Vanderhaeghe and Teyssier,
724 1997; Dalziel and Brown, 1989). The metamorphic peak of upper amphibolite-granulite
725 facies located in different sectors of the CPIMB at about 350 Ma recognized by Renda
726 et al. (2021), could correspond to a metamorphic core complex, however further
727 studies are needed to confirm it.

728

729 **3.3 Gondwanan event (ca. 330 – 300 Ma) in the CPIMB**

730

731 To analyze the Gondwanan event in the CPIMB, it is important to keep in mind the
732 processes described in detail in Section 3. 1) Pangea was assembled in a super-
733 downwelling, 2) the northeastward movement of Gondwana forming part of Pangea, 3)
734 the counterclockwise rotation of Gondwana domains caused by the self-subduction of
735 Pangea, 4) Slab-suction developed on the Gondwana margins facing the Panthalassa
736 Ocean.

737 **Non-peer reviewed EarthArXiv preprint**

738

739 These processes overlapped differently along the CPIMB giving rise to complex
740 structures such as those described by von Gosen (2009). In general, they will respond
741 to contractional tectonics caused by the super-downwelling, but in different sectors they
742 may be conditioned by the other processes.

743 During Gondwanan event the subduction was again established in the margin where
744 was the CPIMB, as in other margins of Pangea during the late Paleozoic. This would
745 be the cause of the magmatism that gave rise to the Paso del Sapo Plutonic Complex
746 (PSPC) in the Middle Pennsylvanian considering that the fluids (mainly water) released
747 from subducted slabs can generate magma partially melting the overlying lower crust
748 (Fig. 9c).

749 Cerredo and López de Luchi (1998) and López de Luchi and Cerredo (2008) pointed
750 out that rocks that belong to Gondwanan event in Río Chico locality (41°15'S, 70°
751 45'W) have a geochemistry that could be inherited from the source (high grade
752 metamorphic basic rocks, metasedimentary rocks or pre-existing S-type igneous
753 rocks).

754 In Taquetrén range, the plutonic rocks of PSPC intrudes with sharp and structurally
755 concordant contacts the LSIMC and presents an ovoid-shaped geometry, elongated in
756 a NW-SE direction, parallel to the regional structural trend (Renda et al., 2021). They
757 have a pervasive foliation caused by processes ranging from magmatic flow to solid-
758 state deformation with respectively ages of 314.1 ± 2.2 Ma and 302.8 ± 2.2 Ma
759 (Section 1).

760 The NW-SE orientation parallel to the regional structural trend of the rocks of PSPC
761 and its foliation, could be due to slab-suction in the subduction zones of Pangea (Fig.

762

763 **Non-peer reviewed EarthArXiv preprint**

764

765 9c). Process of slab-suction determines that both the subducting and overriding plates
766 are forced to drive symmetrically towards the subduction zone (Conrad and Lithgow
767 Bertelloni, 2004; Faccenna et al., 2021). The movement of the margin of Gondwana
768 where was the CPIMB toward the subduction (Figs. 9c) could have facilitated the
769 emplacement of the plutonic rocks of PSPC in previous metamorphic structures and
770 could have determined the N 300°- 330°/50° foliations (with top-to-the-SW tectonic
771 transport direction, according to Renda et al., 2021).

772 As mentioned in Section 1, Centimeter to meter sized metamorphic xenoliths of
773 paragneisses from the LSIMC are common within the granodiorites of PSPC (Renda et
774 al. 2021). In an area between Río Chico-Mamil Choique and Comallo- Paso Flores
775 (between about 40°S and 42° S and between about 69° and 71°W, present geographic
776 coordinates), angular xenoliths of metapsamopelitic rocks of Cushamen Formation,
777 that can reach a meter in length, are within granites, granodiorites and tonalites of
778 Mamil Choique Group (Cerrodo and López de Luchi, 1998; von Gosen, 2009). Angular
779 xenoliths of these paragneisses indicate that the emplacement of the granitoids
780 occurred at high levels of the crust accompanied by brittle fracturing of the country
781 rocks (von Gosen, 2009).

782 On the other hand, in Río Chico there are rocks of the Mamil Choique Group with
783 mylonitic textures and folding of foliation bands (López de Luchi and Cerredo, 2004). In
784 the Sierra de Taquetrén within the PSPC there is a porphyroid granite with marked
785 mylonitic foliation (Section 1). The features observed in both locations indicate, also,
786 ductile deformation.

787 Therefore, it is interpreted that during the Gondwanan event, at least in an area that
788 includes the Taquetrén range and Río Chico-Mamil Choique and Comallo- Paso Flores

789

790 Non-peer reviewed EarthArXiv preprint

791

792 localities, the magma emplacement of the granitoids of PSPC and its correlatable unit,

793 Mamil Choique Group, was accompanied by both ductile and brittle deformation.

794 As mentioned in Section 1, a porphyroid mylonitic granite included in PSPC presents

795 subhorizontal lineations with left and right kinematics indicators that can be associated

796 with the presence of transpressive regime at the time of this emplacement (Renda et

797 al. 2021). Anyway, this is not enough to propose a transpressive deformation with this

798 sole argument. However, this tectonic regime has been recognized by different

799 authors. Martin et al. (1999) proposed a large dextral transpression in the Gondwanan

800 margin of Chile (approximately 39°S present latitude) during the Permian. Von Gosen

801 (2009) pointed out that it can be assumed that the dextral transpression proposed by

802 Martin et al. (1999) also contributed to the directions of compression of the Gondwanan

803 deformation found in the southern border of the North Patagonia Massif. Oriolo et al.

804 (2019) proposed that the Gondwanan deformation (with ages of 299 ± 8 and 302 ± 16

805 Ma) might be essentially linked to transpression in the basement rocks of Challhuaco

806 hill located south of the Nahuel Huapi lake.

807 For von Gosen (2009) the deformation in the southwestern margin of the North

808 Patagonian Massif can be analyzed in conjunction with the late Paleozoic SW-NE

809 compressive deformation in the northeastern sector of this massif. SW-NE direction of

810 compression in the northeast of North Patagonian Massif is also recognized further

811 north in Sierras Australes fold trust belt (von Gosen, 2009). According to von Gosen

812 (2009) to elucidate the kinematic history of Gondwanan deformation, the SW-NE

813 compression seems to have been controlled by South America plate movements. The

814 SW-NE displacement vector represented in Fig. 5 (composed of the northward

815 movement of Gondwana forming part of Pangea and the counterclockwise rotation by

816 the self-subduction of this supercontinent, Section 3) is comparable with the

817 **Non-peer reviewed EarthArXiv preprint**

818

819 compressive directions recognized in different Gondwana localities (see Fig. 14 of von
820 Gosen, 2009).

821 On the other hand, Vizán et al. (2015; 2017) proposed that during the Gondwanan
822 deformation the assemblage of southern Patagonia with the North Patagonian Massif,
823 developed through a dextral transpression, due to the counterclockwise rotation of
824 domains from South America and Africa with respect to domains from India, Australia,
825 Antarctica and southern Patagonia caused by the self-subduction of Pangea in the
826 northern margin of Paleothetys Ocean (Gutiérrez-Alonso et al., 2008; Vizán et al.,
827 2017; Section 3).

828 It was analyzed whether there are geological/structural features that are consistent with
829 this proposal and the transpressive deformation referred above, considering the
830 lineaments that arise from the magnetometric study of Renda et al. (2019). Some of
831 these magnetic lineaments were left aside to make the analysis. Lineaments of the
832 westernmost margin of the North Patagonian Massif with a N-S trend that correspond to
833 structures of the Andean fold and thrust belt (Giacosa and Heredia, 2004) were not
834 considered. Lineaments that correspond to Paleozoic-Mesozoic rifting structures
835 reactivated by Andean tectonics (Gianni et al., 2017) were also left out of this analysis.
836 Then, a pattern of lineaments comparable to that of faults that correspond to the San
837 Andreas System Fault (Nicholson et al., 1986) was recognized (compare Figs. 10a and
838 10b). A strike-slip duplex (Woodcock and Fischer, 1986) could also be interpreted in a
839 zone bounded by the lineaments Río Chubut Medio Fault-Taquetrén Thrust Front
840 (RCMF-TTF) and Piedra Parada Fault (PPF). It is suggested that the NW lineaments

841

842 **Non-peer reviewed EarthArXiv preprint**

843

844 could correspond to strike-slip faults (Fig. 9d). The suggested faults present a pattern
845 similar to the systems proposed by Coira et al. (1975).

846 For von Gosen and Loske (2004) and Zaffarana et al. (2010) there are no trending
847 brittle deformation affecting Jurassic rocks, so the suggested strike-slip faults should be
848 older. The Cisuralian age of the undeformed batholith corresponding to the STPC
849 constrains the age of the suggested strike-slip faults. Perhaps, the age of ca. 303 Ma
850 obtained in PSPC (Section 1) could correspond to the dextral transpressive process
851 that is discussed.

852 The suggested strike-slip faults (Fig. 9d) would have developed during the Gondwanan
853 event in an area that includes the Taquetrén range and Río Chico-Mamil Choique and
854 Comallo- Paso Flores localities. Further to the north-west, close to the Andes mountain
855 range, the metamorphic rocks of Colohuincul Complex recorded a crustal thickening
856 during the Gondwanan event (Oriolo et al., 2019) and its rheological behavior must
857 have been different.

858

859

860

861

862

863

864

865

866

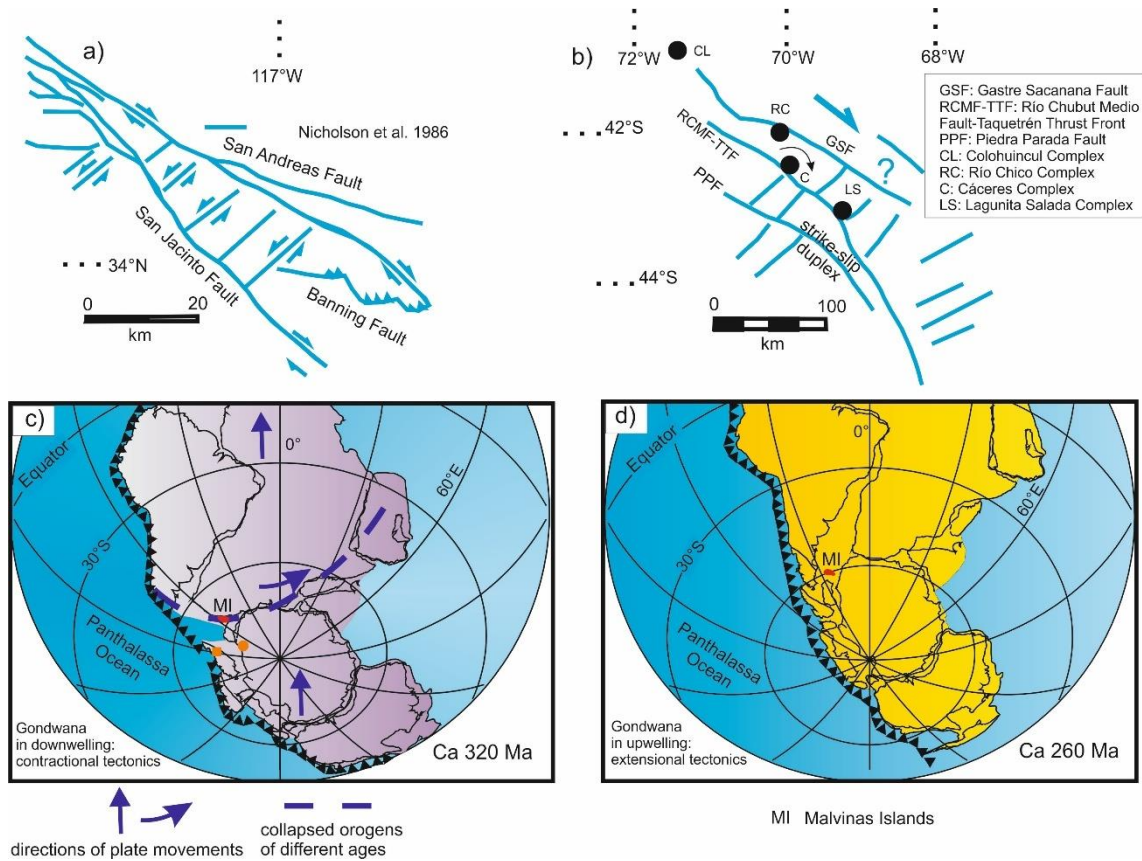
867

868

869 Non-peer reviewed EarthArXiv preprint

870

871



872
873

874

875 **Fig. 10. a) Block model for shear rotation near the intersection of San Andreas**
 876 **and San Jacinto Faults (Southern California) within the San Andreas Fault**
 877 **System (Nicholson et al., 1986). b) Lineaments in the Central Patagonian Igneous**
 878 **Metamorphic Belt, determined through the magnetometric study of Renda et al.**
 879 **(2019). c) and d) paleogeographic reconstructions of Gondwana for the late**
 880 **Carboniferous-late Permian, based on Vizán et al. (2015). The Euler's poles to**
 881 **make the reconstructions of South America, Africa, Australia, Antarctica, India**
 882 **and Arabia are those of Vizán et al. (2015). In Fig. 10c, notice the position of**
 883

884 **Non-peer reviewed EarthArXiv preprint**

885

886 **southern Patagonia respect to South America, reconstructed as explained**
887 **previously in this work. Orange square: Tepuel-Genoa Basin according to**
888 **paleomagnetic reconstruction explained in Section 2 at about 320 Ma. Orange**
889 **circle: Shackleton range.**

890

891 This Permian transpressive deformation zone in South America (Fig. 10c) would
892 connect with the zone of the collapsed East African-Antarctic-Arabian orogen formed
893 during the Neoproterozoic–Cambrian (Stern, 1994; Jacobs and Thomas, 2004). In the
894 weak lithospheric zones that belong to the branches of this collapsed orogen, the
895 “Falkland East Africa Tethys Shear System” (Visser and Praekelt, 1996) was then
896 installed during the late Paleozoic (Fig. 10c).

897 The strike-slip fault system in Patagonia, suggested above, that would continue in
898 South Africa, could have caused clockwise rotations of minor blocks along vertical
899 axes. In this regard, it is discussed whether the Malvinas/Falkland Islands occupied a
900 position southeast of Africa and their present position with respect to South America
901 was acquired by a rotation of more than 150°. There are stratigraphic correlations (Adie
902 1952) together with structural (Curtis and Hyam, 1998) and gravimetric and seismic
903 data (Stanca et al., 2019) that agree with this possibility. For Johnston (2000), the
904 rotation of the Malvinas/Falkland Islands could have occurred in two stages: 1) a
905 clockwise rotation of about 90° along a vertical axis as an additional manifestation of
906 the dextral transpressive character of the Gondwanide deformation in the Cape Fold
907 Belt, 2) a translation of 60-70°, without a rotation along a vertical axis, of the
908 Malvinas/Falkland Islands from South Africa along the Agulhas-Fracture Zone, with
909 development of Jurassic-Cretaceous basins (Schimschal and Jokat, 2019). This last
910 movement can be attributed to the opening of the Atlantic Ocean (Mitchell et al., 1986).

911 **Non-peer reviewed EarthArXiv preprint**

912

913 Therefore, it is interpreted that the Malvinas/Falkland Islands experienced a significant
914 clockwise rotation due to a Gondwanan dextral transpression that assembled the North
915 Patagonian Massif with southern Patagonia (Fig. 10c and 10d) during the Gondwanan
916 event. The proposal of Ramos et al. (2017) indicating that Malvinas/ Falkland Islands
917 were in the present position relative to South America could be valid since the late
918 Permian.

919 In the same way, it was analyzed whether a crustal block could have rotated clockwise
920 in the CPIMB due to the activity of the suggested fault system. While in the Lagunita
921 Salada and Río Chico complexes the azimuths of metamorphic foliation plane is NW-
922 SE, the azimuth of the metamorphic foliation is NNE-SSW in the Cáceres Complex.
923 The NW-SE LSIMC foliation was considered to have the original orientation of when
924 the orogen was built during the Chanic event as mentioned before. Then, it was used
925 as a reference to analyze if the block where the Cáceres Complex is located suffered a
926 rotation along a vertical axis. According to own field measurements, the foliation plane
927 in the Cáceres Complex has an azimuth of 15°. Therefore, if the azimuths of the LSIMC
928 foliations (300°-330°) are taken as references, the block of the Cáceres Complex would
929 have rotated clockwise between 75° and 45°.

930 In Jurassic lithologies of the Cañadón Asfalto Basin that is in the area of the CPIMB,
931 clockwise and counterclockwise rotations of blocks less than 30° were recorded
932 (Geuna et al., 2000; Zaffarana and Somoza, 2012). Since they are not as large as that
933 interpreted for the block with the Cáceres Complex, it is suggested that the latter block
934 could have rotated clockwise during the Permian due to the dextral transpressive
935 movement that attached southern Patagonia to the North Patagonian Massif.

936

937 **Non-peer reviewed EarthArXiv preprint**

938

939 The movement towards the NE of South America (Fig. 5) continued throughout the
940 Gondwanan event (Vizán et al., 2015) and is contrary to what would correspond to the
941 formation of an orogen by advancing subduction in the southern margin of the CPIMB
942 at approximately 300 Ma (e.g., Oriolo et al. 2019). On the other hand, any proposal that
943 indicates a collision of southern Patagonia during Gondwanan event due to its
944 displacement towards South America (e.g., Pankhurst, et al. 2006), would have to
945 prove that this block moved at a speed greater than that indicated by the movement to
946 the NE of South America (Fig.5) greater than 10 cm/year (Table 6).

947

948 As mentioned in Section 1, the last Paleozoic stratigraphic unit outcropping in
949 Taquetrén range is composed by unfoliated granitoids of a non-deformed batholith that
950 according to Renda et al. (2021) has a Permian age of about 290 Ma and it was called
951 Sierra de Taquetrén Plutonic Complex (STPC). Both the LSIMC and PSPC are
952 intruded by the plutonic bodies of this batholith. The undeformed complex constrained
953 the age of late Paleozoic deformations.

954 The rocks of the STPC batholith were emplaced in a context of extensional tectonics
955 (Fig. 9e) caused by the change in the mantle from a super-downwelling to a hot super-
956 upwelling, after 50 million years since Pangea formation (see Section 3).

957

958 **5. Conclusions**

959 In the introduction to this work (Section 1), several questions were raised regarding the
960 tectonic processes that recorded in the CPIMB. Paleogeographic reconstructions
961 based on paleomagnetic data, together with studies carried out in the Taquetrén range

962

963

964 **Non-peer reviewed EarthArXiv preprint**

965

966 added to geological backgrounds proposed by other authors, made possible to answer
967 these questions.

968 From about 400 Ma to about 360 Ma, South America moved from the NE to the SW,
969 and on its southern border, where the CPIMB is located at Present, an accretionary
970 orogen was generated during Chanic event (Fig. 9a). In the Taquetrén range the
971 lithologies of this orogen correspond to the Lagunita Salada Igneous Metamorphic
972 Complex.

973 At the end of this event, South America (as part of Gondwana) abruptly change its
974 direction of drifting and move northward, pulled by a subduction in the boreal margin of
975 the Rheic Ocean. In the CPIMB a magmatic lull is registered during this abrupt change
976 of South American movement. It is interpreted that during this time span (between ca.
977 360 Ma and ca. 340 Ma) took place the collapse of the orogen built during the Chanic
978 event.

979 Gondwana after partially closing the Rheic Ocean at approximately 340 Ma constitutes,
980 together with Laurasia, the Pangea supercontinent. This supercontinent was
981 assembled on top of a super-downwelling what caused the contraction of Pangea and
982 the installation of subduction zones bordering its margins in which slab-suction process
983 developed.

984 During the Gondwanan event (between ca. 330 Ma and ca. 300 Ma), the installation of
985 these subduction zones gave rise to magmatism whose lithologies in the Taquetrén
986 range belong to the Paso del Sapo Plutonic Complex with magmatic and deformational
987 foliations. The emplacement of this complex and its foliations could be conditioned by
988 slab-suction processes.

989

990

991

992

993 **Non-peer reviewed EarthArXiv preprint**

994

995 The emplacement of these rocks was accompanied by ductile and brittle fracturing
996 deformation of the crust in an area that includes the Taquetrén range and Río Chico-
997 Mamil Choique and Comallo- Paso Flores localities.

998 Structural lineaments recognized through a magnetometric study suggest a fault

999 system typical of a dextral transpression. It is suggested that this event attached

1000 southern Patagonia to North Patagonian Massif (Figs. 9d, 10c and 10d) and could have

1001 caused a clockwise rotation of a block with rocks of the interpreted collapsed Chanic

1002 orogen, as well as the Malvinas/Falkland Islands during the Gondwanan event at ca.

1003 300 Ma.

1004 This transpressive process occurred prior to the emplacement of an undeformed

1005 batholith in a context of extensional tectonics at ca. 290 Ma (Fig. 9e).

1006

1007 **Acknowledgements**

1008

1009 This work was supported by UBACyT N° 2002015010069BA. Many thanks to Silvana

1010 E. Geuna, Emiliano M. Renda, Sebastián Oriolo and Silvia L. Lagorio. To the memory

1011 of Rubén.

1012

1013 **References**

1014 Adie, R. J. 1952. The Position of the Falkland Islands in a Reconstruction of

1015 Gondwanaland. Geological Magazine, 89(6), 401- 410.

1016 <https://doi.org/10.1017/S0016756800068102>

1017

1018

1019 **Non-peer reviewed EarthArXiv preprint**

1020

1021 Alvey, A. 2009. Using crustal thickness and continental lithosphere thinning factors
1022 from gravity inversion to refine plate reconstruction models for the Arctic and North
1023 Atlantic. Ph. D. Thesis, Liverpool University (unpublished), 189 p, Liverpool.

1024

1025 Anderson, D.L., 1982. Hotspots, polar wander, Mesozoic convection and the geoid.
1026 Nature 297, 391–393.

1027

1028 Bahadori, A., Holt, W.E., Austermann, J., Campbell, L., Rasbury, E.T., Davis, D.M.,
1029 Calvelage, C.M. and Flesch, L.M., 2022. The role of gravitational body forces in the
1030 development of metamorphic core complexes. Nature Communications 13:564.
1031 <https://doi.org/10.1038/s41467-022-33361-2>.

1032

1033 Bercovici, D., Ricard, Y., Richards, M.A., 2000. The Relation Between Mantle
1034 Dynamics and Plate Tectonics: A Primer. The History and Dynamics of Global Plate
1035 Motions, GEOPHYSICAL MONOGRAPH 121, M. Richards, R. Gordon and R. van der
1036 Hilst, eds., American Geophysical Union, pp.5–46.
1037

1038 Besse, J. and Courtillot, V., 2002. Apparent and true polar wander and the geometry of
1039 the geomagnetic field over the last 200 Myr. Journal of Geophysical Research, Vol.
1040 107, (Nº B11), 1-31. <https://doi.org/10.1029/2000JB000050>.

1041 Bilmes, A., D'Elia, L., Franzese, J.R., Veiga, G.D., Hernández, M., 2013. Miocene
1042 block uplift and basin formation in the Patagonian foreland: the Gastre Basin,
1043 Argentina. Tectonophysics 601 (98), 111. <https://doi.org/10.1016/j.tecto.2013.05.001>.

1044 **Non-peer reviewed EarthArXiv preprint**

1045

1046 Bucher, J., García, M., López, M., Milanese, F., Bilmes, A., D'Elia, L., Naipauer, M.,
1047 Sato, A.M., Funes, D., Rapalini, A., Franzese, J., 2019. Tectonostratigraphic evolution
1048 and timing deformation in the Miocene Paso del Sapo Basin: implications for the
1049 Patagonian Broken Foreland. *J. South Am. Earth Sci.* 94, 102212.

1050

1051 Bullard, E. C., Everett, J. E. and Smith, L G. 1965. The fit of the continents around the
1052 Atlantic. *Philosophical Transactions of the Royal Society, London.* A258. 41- 51.

1053

1054 Calderón, M., Hervé, F., Fuentes, F., Fosdick, J.C., Sepúlveda, F., Galaz, G., 2016.
1055 Tectonic evolution of Paleozoic and Mesozoic Andean metamorphic complexes and
1056 the Rocas Verdes Ophiolites in southern Patagonia. In: Ghiglione, M.C. (Ed.),
1057 *Geodynamic Evolution of the Southernmost Andes.* Springer Earth System Sciences,
1058 pp. 7–36.

1059

1060 Cawood, P.A., Kroner, A., Collins, W.J., Kusky, T.M., Mooney, W.D., Windley, B.F.,
1061 2009. Accretionary orogens through Earth History. *Earth Accretionary Systems in*

1062

1063 *Space and Time.* Cawood, P. A. & Kroner, A. (eds). The Geological Society, London,
1064 *Special Publications*, 318, 1–36.

1065 Cerredo, M.E., López De Luchi, M.G., 1998. Mamil Choique granitoids, southwestern
1066 North Patagonian event, Argentina: magmatism and metamorphism associated with a
1067 polyphasic evolution. *J. South Am. Earth Sci.* 11, 499–515. [https://doi.org/](https://doi.org/10.1016/S0895-9811(98)00025-X)

1068 10.1016/S0895-9811(98)00025-X.

1069

1070 **Non-peer reviewed EarthArXiv preprint**

1071

1072 Coltice, N., Phillips, B.R., Bertrand, H., Ricard, Y., Rey, P., 2007. Global warming of the
1073 mantle at the origin of flood basalts over supercontinents. *Geology* 35, 391–394.

1074 doi:10.1130/G23240A.1

1075

1076 Coira, B.L., Nullo, F.E., Proserpio, C., Ramos, V.A., 1975. Tectónica de basamento de
1077 la región Occidental del Macizo Nordpatagónico, provincias de Río Negro y Chubut.
1078 *Rev. Asoc. Geol. Argent.* 30 (4), 361–383.

1079

1080 Curtis, M.L. and Hyam, D.M., 1998. Late Palaeozoic to Mesozoic structural evolution of
1081 the Falkland Islands: a displaced segment of the Cape Fold Belt. *Journal of the*
1082 *Geological Society, London*, Vol. 155, 115–129.

1083 Chase, C. G., and Sprowl, D.R., 1983. The modern geoid and ancient plate boundaries,
1084 *Earth Planet. Sci. Lett.*, 62, 314–320, doi:10.1016/0012-821X(83)90002-X.

1085

1086 Dalla Salda, L.H., Cingolani C., Varela, R. 1991. El basamento cristalino de la región
1087 nordpatagónica de los lagos Gutiérrez, Mascardi, y Guillermo, Provincia de Río Negro.
1088 *Rev. Asociación Geológica Argentina* 46(3–4):263–276.

1089

1090 Dalla Salda, L.H., Varela, R., Cingolani, C., Aragón, E., 1994. The Río Chico paleozoic
1091 crystalline complex and the evolution of northern Patagonia. *J. South Am. Earth Sci.* 7,
1092 377–386. [https://doi.org/10.1016/0895-9811\(94\)90022-1](https://doi.org/10.1016/0895-9811(94)90022-1).

1093

1094

1095

1096 **Non-peer reviewed EarthArXiv preprint**

1097

1098 Dalziel, I.W.D. and Brown, R.L., 1998. Tectonic denudation of the Darwin metamorphic
1099 core complex in the Andes of Tierra del Fuego, southernmost Chile: Implications for
1100 Cordilleran orogénesis. *Geology*, 17: 699-703.

1101

1102 Dewey, J.F., 1988. Extensional collapse of orogens. *Tectonics*, 7:1123-1139.

1103

1104

1105 Dewey, J.F. and Bird, J.M., 1970. Mountain Belts and New Global Tectonics. *Journal of*
1106 *Geophysical Research* 75(14): 2625-2647.

1107 Dewey, J.F., Ryan, P.D. and Andersen, T.B., 1993. Orogenic uplift and collapse,

1108 crustal thickness, fabrics and metamorphic phase changes: the roles of eclogites. In:

1109 *Magmatic processes and Plate Tectonics* (Prichard, H.M., Alabaster, T., Harris, N.B.

1110 and Neary, C.R. eds.), *Geological Society Special Publication N° 76*: 325-343. YAN 2 & T

1111

1112 Domeier, M., Van der Voo, R., Torsvik, T.H., 2012. Paleomagnetism and Pangea: The
1113 road to reconciliation. *Tectonophysics*, 514–517: 14–43.

1114

1115 Domeier, M. and Torsvik, T.H., 2014. Plate tectonics in the late Paleozoic.

1116 *GeoscienceFrontiers*, 5: 303-350.

1117

1118 Echaurren, A., Folguera, A., Gianni, G., Orts, D., Tassara, A., Encinas, A., Giménez,

1119 M., Valencia, V., 2016. Tectonic evolution of the North Patagonian Andes (41–44 S)

1120 through recognition of syntectonic strata. *Tectonophysics* 677–678, 99–114.

1121

1122

1123 **Non-peer reviewed EarthArXiv preprint**

1124

1125 Fisher, R.A., 1953. Dispersion on a sphere. *Phil. Trans. Roy. Soc. London A*217, 295–

1126 305.

1127

1128

1129 Figari, E.G., 2005. Evolución Tectónica de la Cuenca de Cañadón Asfalto. Tesis

1130 Doctoral 3896, Facultad de Ciencias Exactas y Naturales, Universidad Nacional de

1131 Buenos Aires. Biblioteca Digital FCEN-UBA, 198 pp. (inédito).

1132

1133 Figari, E., Scasso, R., Cúneo, R. and Escapa, I., 2015. Estratigrafía y evolución

1134 geológica de la Cuenca de Cañadón Asfalto, Provincia del Chubut, Argentina. *Latin*

1135 *American Journal of Sedimentology and Basin Analysis*, vo. 22(2): 135-169.

1136 Foix, N., Allard, J.O., Ferreira, M.L., Atencio, M., 2020. Spatio-temporal variations in

1137 the mesozoic sedimentary record, Golfo San Jorge basin (Patagonia, Argentina):

1138 andean vs cratonic sources. *J. S. Am. Earth Sci.* 102464.

1139

1140 Gallo, L. C., Tomezzoli, R. N., and Cristallini, E. O., 2017, A pure dipole analysis of the

1141 of Pangea, *Geochem. Geophys. Geosyst.*, 18, 1499– 1519,

1142 doi:10.1002/2016GC006692.

1143

1144 Geuna, S. E., Somoza, R., Vizán, H., Figari, E. G., Rinaldi, C. A., 2000.

1145 Paleomagnetism of Jurassic and Cretaceous rocks in central Patagonia: a key to

1146 constrain the timing of rotations during the breakup of southwestern Gondwana? *Earth*

1147 *and Planetary Science Letters*, Volume 181, Issue 1-2, p. 145-160. August 2000

1148 DOI:10.1016/S0012-821X(00)00198-9

1149 **Non-peer reviewed EarthArXiv preprint**

1150

1151 Geuna, S.E., Escosteguy, L.D. y Miró R., 2008. Palaeomagnetism of the Late
1152 Devonian–Early Carboniferous Achala Batholith, Córdoba, central Argentina:
1153 Implications for the apparent polar wander path of Gondwana. *Gondwana Research*
1154 13: 227–237.

1155

1156 Giacosa, R.E., 2020. Basement control, sedimentary basin inception and early
1157 evolution of the Mesozoic basins in the Patagonian foreland. *J. S. Am. Earth Sci.*
1158 102407.

1159

1160 Giacosa, R.E., Heredia, C., 2004. Structure of the North Patagonian thick-skinned
1161 foldand-thrust belt, southern central Andes, Argentina (41°-42°S). *J. South Am. Earth*
1162 *Sci* 18, 61–72. <https://doi.org/10.1016/j.jsames.2004.08.006>

1163

1164 Giacosa, R.E., González, P.D., Silva Nieto, D., Busteros, A., Lagorio, S., Rossi, A.,
1165 2014. Complejo Ígneo-Metamórfico Cáceres: Una nueva unidad metamórfica de alto
1166 grado en el basamento de Gastre, Macizo Nordpatagónico (Chubut). XIX Congreso
1167 Geológico Argentino, Tectónica Preandina.

1168

1169 Gianni, G.M., Echaurren, A., Folguera, A., Likerman, J., Encinas, A., García, H.P.A.,
1170 Dal Molin, C., Valencia, V.A., 2017. Cenozoic intraplate tectonics in Central Patagonia:
1171 Record of main Andean phases in a weak upper plate. *Tectonophysics* 721, 151– 166.
1172 <https://doi.org/10.1016/j.tecto.2017.10.005>

1173

1174

1175 **Non-peer reviewed EarthArXiv preprint**

1176

1177 Gurnis, M., 1988. Large-scale mantle convection and the aggregation and dispersal of
1178 supercontinents. *Nature* 332, 695–699.

1179

1180 Gutiérrez-Alonso, G., Fernández Suárez, J., Weil, A., Murphy, B., Nance, D., Corfú, F.,
1181 and Johnston, S., 2008. Self-subduction of the Pangaeen global plate: *Nature*
1182 *Geoscience*, v. 1, p. 549–553, doi: 10.1038/ngeo250 .

1183 Hallam, A., 1983. Supposed Permo-Triassic megashear between Laurasia and

1184 Gondwana. *Nature* 301, 499–502. doi:10.1038/301499a0

1185

1186 Henry, B., Merabet, N.E., Bouabdallah, H., Maouche, S., 1999. Nouveau pôle
1187 paléomagnétique Stéphanien inférieur pour le cratón saharien (formation de Merkala,
1188 bassin de Tindouf, Algérie). *Comptes Rendus de l'Academie des Sciences, Series IIA*
1189 *Earth and Planetary Science*, 329(3), 161-166.

1190 Hopper, E., Fischer, K.M., Wagner, L.S., Hawman, R.B., 2017. Reconstructing the end
1191 of the Appalachian orogeny. *Geology* 45, 15-18.

1192

1193 Irving, E., 1977. Drift of the major continental blocks since the Devonian. *Nature* 270,
1194 304–309 doi:10.1038/270304a0.

1195

1196

1197 Jacobs, J. and Thomas, R.J., 2004. Himalayan-type indenter-escape tectonics model
1198 for the southern part of the late Neoproterozoic–early Paleozoic East African–Antarctic
1199 orogen. *Geology*; v. 32; no. 8; p. 721–724; doi: 10.1130/G20516.1

1200

1201 **Non-peer reviewed EarthArXiv preprint**

1202

1203 Johnston, S.T., 2000. The Cape Fold Belt and Syntaxis and the rotated Falkland
1204 Islands: dextral transpressional tectonics along the southwest margin of Gondwana.
1205 Journal of African Earth Sciences, 31 (1), 1-13.

1206

1207 Kumar, P., Yuan, X., Ravi Kuman, M., Kind, R., Li, X., and Chadha, R.K., 2007, The
1208 rapid drift of the Indian tectonic plate: Nature, v. 449, p. 894–897, doi: 10 .1038
1209 /nature06214.

1210 Lawver, L.A., and Scotese, C.R., 1987, A revised reconstruction of Gondwanaland, *in*
1211 McKenzie, G.D., ed. Gondwana Six: Structure, Tectonics, and Geophysics: American
1212 Geophysical Union Geophysical Monograph 40, p. 17–23, doi: 10 .1029 /GM040p0017.

1213

1214 Li, Z.X. and Zhong, S. 2009. Supercontinent–superplume coupling, true polar wander
1215 and plume mobility: Plate dominance in whole-mantle tectonics. Physics of the Earth
1216 and Planetary Interiors 176: 143–156.

1217 López de Luchi, M. and Cerredo, M.E., 2008. Geochemistry of the Mamil Choique
1218 granitoids at Rio Chico, Río Negro, Argentina: Late Paleozoic crustal melting in the
1219 North Patagonian Massif. Journal of South American Earth Sciences, 25: 526–546.

1220

1221

1222 Marcos, P., Pavón Pivetta, C., Benedini, L., Gregori, D., Geraldés, M., Scivetti, N.,
1223 Barros, M., Varela, M., Costa dos Santos, A., 2020. Late Paleozoic geodynamic
1224 evolution of the western North Patagonian Massif and its tectonic context along the
1225 southwestern Gondwana margin, Lithos, Vol. 376–377,2020,105801,ISSN 0024-
1226 4937,https://doi.org/10.1016/j.lithos.2020.105801.

1227 **Non-peer reviewed EarthArXiv preprint**

1228

1229 Martin, M.W., Kato, T.T., Rodríguez, C., Godoy, E., Duhart, P., McDonough, M.,
1230 Campos, A., 1999. Evolution of the late Paleozoic accretionary complex and overlying
1231 fore-arc magmatic arc, south central Chile (38-41°S): constrained for the tectonic
1232 setting along the southwestern margin of Gondwana. *Tectonics*, 18(4): 582-605.

1233 Maruyama, S., Santosh, M., Zhao, D., 2007. Superplume, supercontinent, and
1234 postperovskite: mantle dynamics and anti-plate tectonics on the core–mantle boundary.
1235 *Gondwana Res.* 11, 7–37.

1236

1237 McElhinny, M.W., Powell, Ch.McA., Pisarevsky, S.A., 2003. Paleozoic terranes of
1238 eastern Australia and the drift history of Gondwana. *Tectonophysics*, 362, 41-65.

1239

1240 Merabet, N., Henry, B., Bouabdallah, H., Maouche, S., 1999. Paleomagnetism of the
1241 Djebel Reouina Namurian Formation (Tindouf Basin, Algeria). *Studia Geophysica et*
1242 *Geodaetica*, 43(4), 376-389.

1243

1244 Merdith, A.S., Williams, S.E, Collins, A.S., Tettley, M.G., Mulder, J.A., Blades, M.A.,
1245 Young, A., Armistead, S.E., Cannon, J., Zahirovic, S., Müller, D., 2021.

1246

1247 Extending full-plate tectonic models into deep time: Linking the Neoproterozoic and the
1248 Phanerozoic. *Earth-Science Reviews* 214, 103477.

1249

1250 Morel, P. e Irving, E. 1981. Paleomagnetism and the evoluion of Pangea. *Journal of*
1251 *Geophysical Research*, vol. 86, no. b3:1858-1872.

1252

1253 **Non-peer reviewed EarthArXiv preprint**

1254

1255 Mundl, A., Ntaflos T., Ackerman L., Bizimis M., Bjerg E.A. y Hauzenberger C.A., 2015.

1256 Mesoproterozoic and Paleoproterozoic subcontinental lithospheric mantle domains

1257 beneath southern Patagonia: Isotopic evidence for its connection to Africa and

1258 Antarctica. *Geology*, 43 (1) 39–42. doi:10.1130/G36344.1.

1259

1260 Mundl, A., Ntaflos, T., Ackerman, L., Bizimis, M., Bjerg, E.A. , Wegner, W. and

1261 Hauzenberger, C.A., 2016. Geochemical and Os–Hf–Nd–Sr Isotopic Characterization

1262 of North Patagonian Mantle Xenoliths: Implications for Extensive Melt Extraction and

1263 Percolation Processes. *Journal of Petrology*, 57 (4): 685–715.

1264

1265 Muttoni, G., Kent, D.V., Garzanti, E., Brack, P., Abrahamsen, N. and Gaetani, M. 2003.

1266 Early Permian Pangea “B” to Late Permian Pangea “A”. *Earth and Planetary Science*

1267 *Letters*, 215: 379-394.

1268

1269 Nance, D., Gutierrez-Alonso, G., Keppie, D., Linnemann U., Murphy, J.B., Quesada,

1270 C., Strachan, R.A. and Woodcock, N.H., 2012. A brief history of the Rheic Ocean.

1271 *Geoscience Frontiers* 3(2): 125-135.

1272

1273 Nicholson, C., Seeber, L., Williams, P. and Sykes, L.R., 1986. Seismic evidence for

1274 conjugate slip and block rotations within the San Andreas fault system, Southern

1275 California. *Tectonics*, Vol. 5, N° 4: 629-648.

1276

1277

1278

1279 **Non-peer reviewed EarthArXiv preprint**

1280

1281 Nokleberg, W., Parfenov, L.M., Monger, J.W., Norton, I.O., Khanchuk, A.I., Stone, D.B.,
1282 Scotese, C.R., Scholl, D.W. and Fujita, K., 2001. Phanerozoic Tectonic Evolution of the
1283 Circum-North Pacific. United State Geological Survey, Professional Paper 1626. 122
1284 pp.

1285

1286 Oriolo, S., Schulz, B., González, P.D., Bechis, F., Olaizola, E., Krause, J., Renda, E.M.
1287 and Vizán, H., 2019. The Late Paleozoic tectonometamorphic evolution of Patagonia
1288 revisited: insights from the pressure-temperature-deformation-time (P-T-D-t) path of the
1289 Gondwanide basement of the north Patagonian Cordillera (Argentina). *Tectonics*, 38:
1290 2378-2400.

1291

1292 Pankhurst, R.J., Rapela, C.W., Fanning, C.M., Márquez, M., 2006. Gondwanide
1293 continental collision and the origin of Patagonia. *Earth Sci. Rev.* 76, 235–257.
1294 <https://doi.org/10.1016/j.earscirev.2006.02.001>.

1295

1296 Pastor Galán, D., Gutiérrez-Alonso, G., Murphy, J.B., Fernández-Suárez, J., Hofmann,
1297 M., Linnemann, U., 2013. Provenance analysis of the Paleozoic sequences of the
1298 northern Gondwana margin in NW Iberia: Passive margin to Variscan collision and
1299 orocline development. *Gondwana Research*, 23: 1089–1103.

1300

1301

1302

1303

1304 **Non-peer reviewed EarthArXiv preprint**

1305

1306 Pastor Galán, D. 2022. From supercontinent to superplate: Late Paleozoic Pangea's
1307 inner deformation suggests it was a short-lived superplate. *Earth-Science Reviews*
1308 226, 103918.

1309

1310 Ramos, V.A., 2008. Patagonia: a Paleozoic continent adrift? *J. S. Am. Earth Sci.* 26,
1311 235–251.

1312

1313 Ramos, V.A., Cingolani, C., Chemale, F., Naipauer, M., Rapalini, A., 2017. The
1314 Malvinas (Falkland) Islands revisited: The tectonic evolution of southern Gondwana
1315 based on U-Pb and Lu-Hf detrital zircon isotopes in the Paleozoic cover. *Journal of*
1316 *South America Earth Sciences*, 76, 7: 320-345.

1317 Rapalini, A., Tarling, D., Turner, P., Flint, S. F., Vilas, J., 1994. Paleomagnetism of the
1318 Carboniferous Tepuel Group, Central Patagonia, Argentina. *Tectonics*. 13: 1277-1294.
1319 doi: 10.1029/94TC00799.

1320

1321

1322 Ravazzoli, I.A., Sesana, F.L., 1977. Descripción geológica de la Hoja 41c "río Chico"
1323 (1: 200.000), provincia de Río negro. Servicio Geológico Nacional, Boletín N° 148, 1–
1324 77.

1325

1326 Reilinger, R., McClusky, S., Vernant, P., Lawrence, S., Ergintav, S., Cakmak, R.,
1327 Ozener, H., Kadirov, F., Guliev, I., Stepanyan, R., Nadariya, M., Hahubia, G.,
1328 Mahmoud, S., Sakr, K., ArRajehi, A., Paradissis, D., Al-Aydrus, A., Prilepin, M., Guseva,
1329 T., Evren, E., Dmitrova, A., Filikov, S.V., Gomez, F., Al-Ghazzi, R., Karam, G., 2006.

1330 **Non-peer reviewed EarthArXiv preprint**

1331

1332 GPS constraints on continental deformation in the Africa–Arabia–Eurasia continental
1333 collision zone and implications for the dynamics of plate interactions. *Journal of*
1334 *Geophysical Research* 111, B05411, <http://dx.doi.org/10.1029/2005JB004051>.

1335 Renda, E.M., 2020. Estudios geológicos y geofísicos a lo largo de una faja de
1336 deformación entre dominios patagónicos; la sierra de Taquetrén. Tesis Doctoral.
1337 Facultad de Ciencias Exactas y Naturales. Universidad de Buenos Aires. 292 pp.

1338

1339 Renda, E. M., Álvarez, M.D., Prezzi, C., Oriolo, S. y Vizán, H., 2019. Inherited
1340 basement structures and their influence in foreland evolution: A case study in Central
1341 Patagonia, Argentina. *Tectonophysics*, 772: 228-232.

1342

1343 Renda, E.M., González, P.D., Vizán, H., Oriolo, S., Prezzi, C.B., Ruiz-González, V.,
1344 Schulz, B., Krause, J., Basei, M., 2021. Igneous-metamorphic basement of Taquetrén
1345 Range, Patagonia, Argentina: A key locality for the reconstruction of the Paleozoic
1346 evolution of Patagonia. *Journal of South American Earth Sciences* 106, 103045

1347

1348 Rey P, Vanderhaeghe O., Teyssier C., 2001. Gravitational collapse of the continental
1349 crust: definition, regimes and modes. *Tectonophysics* 342:3–4.

1350

1351 Rojo D., Calderón M., Hervé F., Díaz J., Quezada P., Suárez R., Ghiglione M., F.,
1352 Fuentes F., Theye T., Cataldo J., Sandoval J., Viefhausi T., 2021. Petrology and
1353 tectonic evolution of late Paleozoic mafic-ultramafic sequences and the Leones Pluton
1354 of the Eastern Andean Metamorphic Complex (46-47°S), southern Chile. *Journal of*
1355 *South American Earth Sciences* 108, 103198

1356

1357 **Non-peer reviewed EarthArXiv preprint**

1358

1359 Royden, L.H., 1993. The tectonic expression slab pull at the continental convergent
1360 boundaries. *Tectonics*, 12 (2): 303-325.

1361 Ruiz González, V., Puigdomenech, C.G., Zaffarana, C.B., Vizán, H., Somoza, R., 2020.
1362 Paleomagnetic evidence of the brittle deformation of the central Patagonian batholith at
1363 Gastre area (Chubut province, Argentina). *J. S. Am. Earth Sci.* 98, 102442

1364

1365 Santosh, M., Maruyama, S., Yamamoto, S., 2009. The making and breaking of
1366 supercontinents: some speculations based on superplumes, super-downwelling and
1367 the role of tectosphere. *Gondwana Res.* 15, 324–341.

1368

1369 Serra-Varela, S., Heredia, N., Giacosa, R., García Sansegundo, S. y Farias, P., 2020.
1370 Review of the polyorogenic Palaeozoic basement of the Argentinean North Patagonian
1371 Andes: age, correlations, tectonostratigraphic interpretation and geodynamic evolution,
1372 *International Geology Review*, DOI: 10.1080/00206814.2020.1839798

1373 Schimschal, C.M. and Jokat, W., 2019. The Falkland Plateau in the context of
1374 Gondwana breakup. *Gondwana Research*, 68: 108-115.

1375

1376 Scotese, C.R., 2001, *Atlas of Earth History 1. Paleogeography: PALEOMAP Project*:
1377 Arlington, University of Texas, Department of Geology, 52 p.

1378

1379 Sears, J.W., 2012. Transforming Siberia along the Laurussian margin. *Geology*, 40 (6):
1380 535–538; doi:10.1130/G32952.1

1381

1382

1383 **Non-peer reviewed EarthArXiv preprint**

1384

1385 Senshu, H., Maruyama, S., Rino, S. and Santosh, M., 2009. Role of tonalite–
1386 trondhjemite–granite (TTG) crust subduction on the mechanism of supercontinent
1387 breakup. *Gondwana Res.* 15, 433–442.

1388

1389 Stanca R.M., Paton D.A., Hodgson D.M., McCarthy D.J. y Mortimer D.J., 2019. A
1390 revised position for the rotated Falkland Islands microplate. *Journal of the Geological*
1391 *Society*, doi: 10.1144/jgs2018-163.

1392

1393 Stern, R.J., 1994. Arc assembly and continental collision in the Neoproterozoic East
1394 African Orogen: Implications for the consolidation of Gondwana. *Annu. Rev. Earth*
1395 *Planet. Sci.*, 22:319-51.

1396

1397 Suárez, R., González, P.D., Ghiglione, M.C., 2019. A review on the tectonic evolution
1398 of the Paleozoic-Triassic basins from Patagonia: record of protracted westward
1399 migration of the pre-Jurassic subduction zone. *J. S. Am. Earth Sci.* 102256.

1400

1401 Taboada, A. C. and Shi, G. R. 2011, Taxonomic review and evolutionary trends of
1402 *Levipustulini* and *Absenticostini* (Brachiopoda) from Argentina: palaeobiogeographic
1403 and palaeoclimatic implications, *Memoirs of the Association of Australasian*
1404 *Palaeontologists*, 41, 87-114.

1405

1406 Taboada, A.C., Peixoto Neves, J., Weinschütz, L.C., Pagani, M.A., Guimarães,
1407 Simões, M., 2016. *Eurydesma–Lyonia* fauna (EarlyPermian) from the *tatararég* group,
1408

1409 **Non-peer reviewed EarthArXiv preprint**

1410

1411 Paraná Basin (Brazil): A paleobiogeographic W–E trans-Gondwanan marine
1412 connection. *Palaeogeography, Palaeoclimatology, Palaeoecology*, 449: 431–454.

1413

1414 Torsvik, T.H., Van der Voo, R., Preeden, U., Mac Niocaill, C., Steinberger, B.,
1415 Doubrovine, P.V., van Hinsbergen, D.J., Domeier, M., Gaina, C., Tohver, T., Meert,
1416 J.G., McCausland, P.J.A., and Cocks, R.M., 2012, Phanerozoic polar wander,
1417 palaeogeography and dynamics: *Earth-Science Reviews*, v. 114, p. 325–368, doi: 10
1418 .1016 /j .earscrev .2012 .06 .007.

1419

1420 Vanderhaeghe, O. and Teyssier, C., 1997. Formation of the Shuswap metamorphic
1421 core complex during late-orogenic collapse of the Canadian Cordillera: Role of ductile
1422 thinning and partial melting of the mid-to lower crust. *Geodinamica Acta*, 10, 2: 41-58.

1423

1424 Van der Voo, R., 1993. *Paleomagnetism of the Atlantic, Tethys and Iapetus Oceans*.
1425 New York, Cambridge University Press, 411pp.

1426

1427 Van der Voo, R., and French, R. B., 1974, Apparent polar wandering for the Atlantic
1428 bordering continents: Late Carboniferous to Eocene: *Earth-Sci. Rev.*, v. 10, p. 99-119.

1429

1430 Van der Voo, R., Mauk, F. J., French, R. B., 1976, Permian-Triassic continental
1431 configurations and the origin of the Gulf of Mexico. *Geology*: 177-180.

1432

1433

1434

1435 **Non-peer reviewed EarthArXiv preprint**

1436

1437 Varela, R., Basei, M.A.S., Cingolani, C.A., Siga Jr., O., Passarelli, C.R., 2005. El
1438 Basamento Cristalino de los Andes norpatagónicos en Argentina: geocronología e
1439 interpretación tectónica. *Rev. Geol. Chile* 32, 167–182.

1440

1441 Varela, R., Gregori, D.A., González, P.D., Basei, M.A.S., 2015. Caracterización
1442 geoquímica del magmatismo de arco Devónico y Carbonífero-Pérmico en el Noroeste
1443 de Patagonia. *Rev. Asoc. Geol. Argent.* 72, 419–43

1444

1445 Visser, J.N.J., and Praekelt, H.E., 1996, Subduction, mega-shear systems and Late
1446 Palaeozoic basin development in the African segment of Gondwana. *Geologische*
1447 *Rundschau*, v. 85, p. 632–646, doi: 10.1007/BF02440101.

1448

1449 Vizán, H., Prezzi, C., Japas, M.S., Van Zele, M.A., Guena, S.E. and Renda E.M., 2015.
1450 Tracción de losa en el margen boreal del océano Paleotetis y deformación en el
1451 interior de Gondwana (incluyendo el cordón plegado de Ventana). *Revista de la*
1452 *Asociación Geológica Argentina*, 72 (3): 355 – 377.

1453

1454 Vizán, H., Prezzi, C., Geuna, S., Japas, M.S., Renda, E., Franzese, J. and Van Zele,
1455 M.A. 2017. Palaeotethys slab pull, self-lubricated weak lithospheric zones, poloidal and
1456 toroidal plate motions and Gondwana tectonics. *Geosphere*, 13(5), doi:
1457 10.1130/GES01444.1.

1458

1459

1460

1461 **Non-peer reviewed EarthArXiv preprint**

1462

1463 Volkheimer, W., 1964. Estratigrafía de la zona extraandina del Departamento de
1464 Cushamen (Chubut) entre los paralelos 42° y 42° 30' y los meridianos 70° y 72°. Rev.
1465 Asoc. Geol. Argent. 19 (2), 85–107.

1466

1467 von Gosen, W., 2009. Stages of Late Palaeozoic deformation and intrusive activity in
1468 the western part of the North Patagonian Massif (southern Argentina) and their
1469 geotectonic implications. Geological Magazine, 146(1): 48-71.

1470

1471 von Gosen, W., and Loske, W., 2004, Tectonic history of the Calcatapul Formation,
1472 Chubut province, Argentina, and the “Gastre fault system”: Journal of South American
1473 Earth Sciences, v. 18, p. 73–88, doi:10.1016/j.jsames.2004.08.007

1474

1475 Vouchez, A., Tommasi A., Mainprice D., 2012. Faults (shear zones) in the Earth's
1476 mantle. Tectonophysics 558-559, 1–27

1477

1478 Weil, A.B., Van der Voo, R., van der Pluijm, B.A., 2001. Oroclinal bending and evidence
1479 against the Pangea megashear: The Cantabria-Asturias arc (northern Spain), Geology;
1480 v. 29; no. 11; p. 991–994.

1481

1482 Woodcock, N.H. and Fischer, M., 1986. Strike-slip duplexes. Journal of Structural
1483 Geology, 8 (7): 725-735.

1484

1485

1486

1487

1488 **Non-peer reviewed EarthArXiv preprint**

1489

1490 Yoshida, M. and Santosh, M., 2011. Supercontinents, mantle dynamics and plate
1491 tectonics: A perspective based on conceptual vs. numerical models. *Earth-Science*
1492 *Reviews*, 105: 1–24.

1493

1494

1495 Zaffarana, C.B.; Somoza, R., 2012. Palaeomagnetism and $^{40}\text{Ar}/^{39}\text{Ar}$ dating from
1496 Lower Jurassic rocks in Gastre, central Patagonia: Further data to explore
1497 tectonomagmatic events associated with the break-up of Gondwana. *Journal of the*
1498 *Geological Society*. 169(4):371-379.

1499 Zaffarana, C.B., López de Luchi, M.G., Somoza, R., Mercader, R., Giacosa, R., and
1500 Martino, R.D., 2010, Anisotropy of magnetic susceptibility study in two classical
1501 localities of the Gastre Fault System, central Patagonia: *Journal of South American*
1502 *Earth Sciences*, v. 30, p. 151– 166, doi:10.1016/j.jsames.2010.10.003.

1503 Zaffarana, C.B., Somoza, R., Orts, D.L., Mercader, R., Boltshauser, B., González, V.R.,
1504 Puigdomenech, C., 2017. Internal structure of the Late Triassic Central Patagonian
1505 batholith at Gastre, southern Argentina: implications for pluton emplacement and the
1506 Gastre fault system. *Geosphere* 13, 1973–1992. <https://doi.org/10.1130/GES01493.1>.

1507

1508 Zhang, N., Zhong, S., Leng, W. and Li, Z.X., 2010. A model for the evolution of the
1509 Earth's mantle structure since the Early Paleozoic. *J. Geophys. Res.*, 115, B06401,
1510 doi:10.1029/2009JB006896.

1511

1512

1513

1514 **Non-peer reviewed EarthArXiv preprint**

1515

1516 Zhong, S., Zhang, N., Zheng-Xiang Li, Z.X., and Roberts, J.H., 2007, Supercontinent
1517 cycles, true polar wander, and very long-wavelength mantle convection. Earth and
1518 Planetary Science Letters, 261: 551–564, doi: 10.1016/j.epsl.2007.07.049 .

1519

1520

1521

1522

1523

1524

1525

1526

1527

1528

1529

1530

1531

1532

1533

1534

1535

1536

1537

1538

1539

1540

1541

1542

1543

1544

1545

1546

1547

1548

1549

1550

1551

1552

1553

1554

1555 **Non-peer reviewed EarthArXiv preprint**

1556

1557 **Tables**

1558 **Table 1: Selected paleomagnetic poles of continents that constituted Gondwana.**

1559 **P. Lon.:** longitude of each paleomagnetic pole. **P. Lat:** latitude of each

1560 **paleomagnetic pole. GPDB: Global Paleomagnetic Data Base**

1561

Stratigraphical unit or locality	Age (Ma)	P.Long.	P. Lat.	Author(s) or GPDB code
Herrada Member, S. Grande (Argentina)	417	9.38°E	43.1° S	GPDB 2639, 6904
Air Intrusives, Niger (África)	407	8.6° E	43.4° S	GPDB 1364, 485
SnowyRiverVolcanics, (Australia)	404	14.54°E	55.04° S	GPDB 1365, 486
LeyshonDevonianDykes, (Australia)	398	22.96°E	55.04° S	GPDB 3262, 8404

Non-peer reviewed EarthArXiv preprint				
Picos and Passagem Series, (Brasil)	390	22.96°E	19.16° S	GPDB 613, 3135
Parke Siltstone, (Australia)	384	17.6° E	29.73° S	GPDB 2574, 6650
Comerong Volcanics, (Australia)	377	1.8° E	15.13° S	GPDB 1565, 1003
Griotte Limestone, Algeria (Africa)	370	19.0° E	21.0° S	GPDB 2725, 7086
Beni-Zireg Limestone, Morocco (Africa)	370	19.8° E	19.2° S	GPDB 2521, 6480

Non-peer reviewed EarthArXiv preprint				
CanningBasinReefs (Australia)	368	15.53°E	1.57° N	GPMDB 1345, 452
CanningBasinReefs 2 (Australia)	368	8.71°E	12.24° S	GPMDB 2942, 7659
BrewerConglomerate, (Australia)	365	17.56° E	3.4° N	GPMDB 2726, 7089
Hervey Group, (Australia)	365	7.64° E	4.68° S	GPMDB 1579, 1031
Mt. Eclipse Sandstone, (Australia)	345	27.22° E	12.00° N	GPMDB 2866, 7471

Non-peer reviewed EarthArXiv preprint Oued Draa AftezLimestone, Moroco, (Africa)	342	52.5° E	7.6° S	GPDB 1080, 2039
Djebel Hadid Red Beds, Moroco, (Africa)	342	56.4° E	0.10° N	GPDB 1080, 2040
BathurstBatholith, (Australia)	330	38.59°E	0.4° S	GPDB 3264, 8405
Basalts, Diorite and contact, Moroco (Africa)	330	62.5° E	16.1° S	GPDB 1080, 2038
Upper Clifden Fm./Lower Rocky Creek (Australia)	325	45.2° E	13.5° S	GPDB 3463, 8818
Connors Volcanics, (Australia)	325	50.1° E	13.2° S	GPMDDB 3265, 8406

Non-peer reviewed EarthArXiv preprint				
Ain EchChebbe, Morocco (Africa)	320	67.0° E	25.0° S	GPDB 181, 3205
Newcastle Range Volcanics, (Australia)	320	42.7° E	34.4° S	GPDB 3561, 9056
Ain EchChebbe, Reggane Basin, Algeria (Africa)	320	56.9° E	28.4° S	GPDB 3402, 8653
Djebel Reouina, Reggane Basin, Algeria (Africa)	320	56.6° E	32.4° S	Merabet et al., (1999)
Abu Durba Sediments, Egipto, (Africa)	308	64.0° E	25.6° S	GPDB 2784, 7224
Merkala Fm., Tindouf Basin, Algeria, (Africa)	307	44.7° E	26.6° S	Henry et al., (1999)

Non-peer reviewed EarthArXiv preprint				
Dwyka System, Tanzania-Zimbabwe, (Africa)	305	45.0° E	25.0° S	GPDB 3489, 8894

1562
1563

1564

1565

1566

1567

1568

1569

1570

1571

1572

1573

1574

1575

1576 **Non-peer reviewed EarthArXiv preprint**

1577

1578 **Table 2: Paleomagnetic Poles of Laurasia Continents between 335 and 330 Ma.**

1579 **P. Lon.:** longitude of each paleomagnetic pole. **P. Lat:** latitude of each

1580 **paleomagnetic pole. GPDB:** Global Paleomagnetic Data Base

Stratigraphical unit or locality	Age (Ma)	P.Lon.	P.Lat.	Author(s) or GPDB code
Deer Lake Fm (USA)	335	304.2 °E	18.6 °S	Billardelo and Kodama (2010)
Jeffreys VillageMm. (USA)	333	309.8 °E	17.8 °S	1534
New BrunswickVolc. (USA)	330	315.18 °E	19.5 °S	Seguin et al. (1985)
Burntisland Kinghorn (UK)	332	332 °E	14 °S	2447
Derbyshire Lavas (UK)	335	335.9 °E	14.13 °S	2440

1581

1582 **The average of these 5 PPs has the following geographic coordinates (in**

1583 **North American coordinates) and statistical parameters (Fisher, 1953): Lat. (°S)=**

1584 **19.56, Lon.(°E)= 309.0, A95(°)= 4.2, K= 327.34**

1585 **Non-peer reviewed EarthArXiv preprint**

1586 **Table 3: Mean paleomagnetic poles of Gondwana in present geographic**

1587 **coordinates of Africa and their mean ages.**

1588 **In parentheses: number of ages averaged to calculate the mean for each mean**

1589 **paleomagnetic pole. N: number of averaged PPs. A₉₅: 95% interval of confidence**

1590 **(Fisher, 1953). K: Fisher's (1953) statistical parameter.**

Ages (Ma)	P. Lon.	P. Lat.	N	A₉₅	K
406.5 (4)					
407.5 (2)	13.51°E	48.13°S	4	8.3°	123.98
378.2 (5)					
380(2)	14.23°E	20.97°S	5	8.4°	83.98
362.2 (5)					
356.5 (2)	15.3 °E	0.01°N	5	11.4°	45.83
332.2 (6)	50.83°E		6		34.13
333.5 (2)		3.02°S		11.6°	
314.3 (7)					
312.5 (2)	53.95°E	28.79°S	7	7.0°	75.32

1591

1592

1593 **Non-peer reviewed EarthArXiv preprint**

1594 **Table 4: Reconstruction parameters (Euler's poles) for paleogeographic**
 1595 **reconstructions of Africa (Gondwana). "zero-longitude Africa method" (Africa**
 1596 **was able to remain quasi- stationary with respect to its longitude). In**
 1597 **parentheses: number of ages averaged to calculate the mean for each time.**

Ages (Ma)	Lat.	Lon.	Rotation angle
406.5 (4) 407.5 (2)	0°	103.51°E	41.87°
378.2 (5) 380(2)	0°	104.23°E	69.03°
362.2 (5) 356.5 (2)	0°	105.3°E	90.01°
332.2 (6) 333.5 (2)	0°	140.83° E	86.98°
314.3 (7) 312.5 (2)	0°	143.95° E	61.21°

--	--	--	--

1598 **Non-peer reviewed EarthArXiv preprint**

1599 **Table 5: Reconstruction parameters (Euler's poles) for reconstructions of South**
 1600 **America (considering Africa quasi- stationary with respect to its longitude). In**
 1601 **parentheses: number of ages averaged to calculate the mean for each time.**

Ages (Ma)	Lat.	Lon.	Rotation angle
406.5 (4) 407.5 (2)	33.84° N	27.19° E	50.82 °
378.2 (5) 380(2)	17.4°N	51.00° E	61.39°
362.2 (5) 356.5 (2)	7.81° N	62.47° E	74.6°
332.2 (6) 333.5 (2)	26.59°N	103.77°E	59.82°
314.3 (7) 312.5 (2)	49.12° N	91.72°E	44.6°

1602 **Non-peer reviewed EarthArXiv preprint**

1603

1604 **Table 6: Speeds of movement of Taquetrén range locality over time.**

1605 **Taking the average age of all those corresponding to the selected paleomagnetic**
1606 **poles of each group.**

1607 Velocities (cm/year):

1608 Between 406.5 and 378.2 Ma: 10.67.

1609 Between 362.2 and 332.3 Ma: 18.29

1610 Between 332.2 and 314.3 Ma: 14.03

1611 **Taking the average age between the oldest and the youngest of the selected**
1612 **paleomagnetic poles of each group:**

1613 Velocities (cm/year):

1614 Between 407.5 and 380 Ma: 10.98

1615 Between 380 and 356.5 Ma: 9.93

1616 Between 356.5 and 333.5 Ma: 23.77

1617 Between 333.5 and 312.5 Ma: 12.03

1618